NATIONAL ENERGY TECHNOLOGY LABORATORY

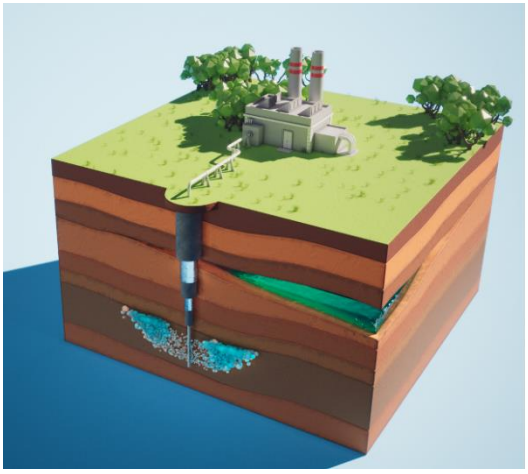

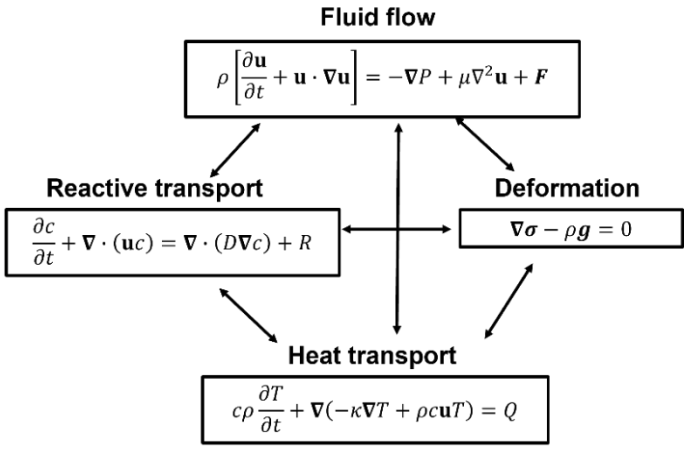

A Brief Overview of Reactive Transport Codes Used in CO_2 Applications

9 September 2022

U.S. DEPARTMENT OF ENERGY | NATIONAL ENERGY TECHNOLOGY LABORATORY

Office of Fossil Energy and Carbon Management

DOE/NETL-2022/3733

Disclaimer

This project was funded by the United States Department of Energy, National Energy Technology Laboratory, in part, through a site support contract.

Cover Illustration: Schematic showing the relationship between reactive transport modeling and environmental and energy systems.

Suggested Citation: Tafen, D. N.; Kutchko, B.; Massoudi, M. *A Brief Overview of Reactive Transport Codes Used in CO_2 Applications*; DOE.NETL-2022.3733; NETL Technical Report Series; U.S. Department of Energy, National Energy Technology Laboratory: Albany, OR, 2022; p 60. DOI: https://doi.org/10.2172/1886680

An electronic version of this report can be found at:

https://netl.doe.gov/energy-analysis

A Brief Overview of Reactive Transport Codes Used in CO_2 Applications

De Nyago Tafen[1,3], Barbara Kutchko[2] , Mehrdad Massoudi[2]

[1]National Energy Technology Laboratory, 1450 Queen Avenue SW, Albany, OR 97321, USA

[2]National Energy Technology Laboratory, 626 Cochran Mill Road, Pittsburgh, PA 15236, USA

[3]NETL Support Contractor, 1450 Queen Avenue SW, Albany, OR 97321, USA

DOE/NETL-2022/3733

9 September 2022

NETL Contacts:

Barbara Kutchko, Principal Investigator

Dustin Crandall, Technical Portfolio Lead

Bryan Morreale, Associate Laboratory Director for Research & Innovation, Research & Innovation Center

This page intentionally left blank.

Table of Contents

List of Figures

List of Tables

Acronyms, Abbreviations, and Symbols

Term	Description
BGK	Bhatnagar-Gross-Krook
CO_2	Carbon dioxide
CCUS	CO_2 capture, utilization, and storage
CFD	Computational fluid dynamics
CST	Continuous species transfer
DOE	U.S. Department of Energy
EOS	Equation of state
LANL	Los Alamos National Laboratory
LBM	Lattice Boltzmann method
LBNL	Laurence Berkeley National Laboratory
LGM	Lattice gas model
MTBE	Methyl tertiary butyl ether
NAPL	Nonaqueous phase liquid
NETL	National Energy Technology Laboratory
OGS	OpenGeoSys
ORNL	Oak Ridge National Laboratory
PNNL	Pacific Northwest National Lab
REV	Representative volume
SNL	Sandia National Laboratory
SPH	Smoothed particle hydrodynamics
STOMP	Subsurface Transport Over Multiple Phases
THMC	Thermo-hydro-mechanical-chemical
VOF	Volume of fluid
Roman Symbols	
A_s^j	Reactive surface of mineral j
c_γ	Specific heat or heat capacity of phase γ
C	Solute concentration
C^j	Concentration of component, species, or particle j
C_γ	Solute concentration in phase γ
C_γ^j	Concentration of component j in phase γ
D	Diffusion coefficient

Acronyms, Abbreviations, Symbols (cont.)

Term	Description
Roman Symbols	
D^j	Diffusion coefficient of particle, component, or species j
D_γ	Diffusivity/Diffusion coefficient of phase γ
$\boldsymbol{D}_\gamma$	Diffusion - dispersion tensor for the phase γ
D_γ^j	Diffusion coefficient of component j for phase γ
$\boldsymbol{D}_\gamma^j$	Diffusion-dispersion tensor of component j for phase γ
D_γ^C	Solute diffusion coefficient for phase γ
D_γ^S	Salt diffusion coefficient for phase γ
$\boldsymbol{D}_{h_\gamma}$	Hydraulic dispersion tensor for phase γ
$\boldsymbol{F}_l^S$	Osmotic flux of the aqueous phase
$\boldsymbol{F}_\gamma^j$	Advective flux of component j in phase γ
g	Gravitational acceleration
h^j	Enthalpy of component j
h_γ	Enthalpy of phase γ
$\boldsymbol{J}_\mathrm{g}^j$	Diffusive-dispersive flux of component j for the gas phase
$\boldsymbol{J}_l^j$	Diffusive-dispersive flux of component j for the liquid phase
$\boldsymbol{J}_n^j$	Diffusive-dispersive flux of component j for the NAPL phase
$\boldsymbol{J}_\gamma^S$	Pressure dispersion flux of salt for phase γ
$k_{r\gamma}$	Relative permeability of phase γ
$\boldsymbol{k}$	Intrinsic permeability tensor
m^j	Mass of particle j
$\dot{m}^j$	Mass source rate of component j
$\dot{m}^C$	Solute rate
$\dot{m}^S$	Salt mass source rate
$\dot{m}_s^i$	Rate of changes for solid mineral i
M^j	Molecular weight of component j
M_γ	Molecular weight of phase γ
$P;\ P^j$	Pressure (particle or component j)
P_γ	Pressure of phase γ
$\dot{q}$	Thermal energy source

Acronyms, Abbreviations, Symbols (cont.)

Term	Description
Roman Symbols	
Q^j	Source / sink of component j
Q_γ^j	Source / sink of component j in phase γ
$\dot{R}^C$	Solute decay rate constant
S	Salt concentration
S_γ	Salt concentration in phase γ
s_γ	Saturation of phase γ
t	Time
T	Temperature
$\mathbf{u}$; $\mathbf{u}^i$	Fluid velocity; velocity of particle i
u_γ	Internal energy of phase γ
u_s	Porous media internal energy
$\mathbf{V}_\gamma$	Darcy velocity vector of phase γ
Y_s^i	Volume fraction of mineral i
$\mathbf{z}_g$	Unit gravitational direction vector
Greek Symbols	
κ	Thermal conductivity
$\boldsymbol{\kappa}_e$	Equivalent thermal conductivity tensor
μ_γ	Kinematic viscosity of phase γ
ρ; ρ^j	Density; density of component or particle j
ρ_γ	Phase density for phase γ
ρ_s	Porous media grain density
ρ_s^i	Density of solid mineral i
τ	Medium tortuosity
$\boldsymbol{\tau}_\gamma$	Phase tortuosity for phase γ
ϕ	Porosity
ϕ_D; ϕ_T	Porosity (diffusive, total)
χ_γ^j	Mole fraction of component j in phase γ
ψ_γ^j	Total concentration of component j in phase γ
ω_γ^j	Mass fraction of component j in phase γ

Acronyms, Abbreviations, Symbols (cont.)

Term	Description
Subscripts	
g	Gas phase
ic	Ice phase
l	Aqueous/liquid phase
n	Nonaqueous phase liquid (NAPL)
s	Rock/soil or solid phase
γ	Generic phase or phase index
Superscripts	
a	Air component
j	Generic component or component index
k	Generic component
o	Oil component
w	Water component

Acknowledgments

This work was completed at the National Energy Technology Laboratory (NETL) with support from U.S. Department of Energy's (DOE) Office of Fossil Energy and Carbon Management. The authors wish to acknowledge Bryan Morreale (NETL Research & Innovation Center), Mark McKoy (NETL Technology Development and Integration Center), and Darin Damiani (DOE Office of Fossil Energy) for programmatic guidance, direction, and support.

This page intentionally left blank.

ABSTRACT

Reactive transport modelling consists of computational and numerical models that describe the coupled physical, chemical, mechanical, and biological processes interacting with each other over a broad range of spatial and temporal scales. This report reviews some of the reactive transport codes available in the literature for carbon dioxide (CO_2) applications and can assist the scientific community with the applicability of each code to solve a specific problem. Approaches implemented in these codes can be categorized in three groups: (i) continuum-scale, (ii) pore-scale, and (iii) hybrid-scale approaches. Theoretical foundations, numerical implementations, and application examples using the models are described. In the continuum approach, flow and transport are formulated in terms of a representative control volume of the medium and coupled with geochemical reactions. The medium is characterized by bulk parameters such as porosity, permeability, or reactive surface area. In the pore-scale approach, each point of space in the pore network is occupied by either a fluid or solid phase. The pore-scale approach requires an exact knowledge of the spatial and temporal phase distribution. In the hybrid-scale approach, media are described by multiple characteristic length-scales, with some regions using a pore-scale approach while others used a continuum approach.

1. INTRODUCTION

The last decades have seen significant advances in tools and approaches for simulating subsurface processes involving flow, transport, and geochemical reactions (Steefel et al., 2015). Reactive transport modelling consists of computational and numerical models that describe the coupled physical, chemical, mechanical, and biological processes interacting with each other over a broad range of spatial and temporal scales. These processes include: (i) multiphase flow (aqueous phase, gaseous phase, super critical phase, non-aqueous phase liquids, etc.); (ii) thermal transport; (iii) geo-mechanics (displacement and deformation); and (iv) biogeochemistry (aqueous complexation, adsorption-desorption, ion-exchange, dissolution-precipitation, surface complexation, acid-base reactions, microbial-mediated redox, etc.). Application fields of reactive transport modelling include geological carbon dioxide storage (Bildstein et al., 2010; DePaolo and Cole, 2013; Gaus et al., 2005), nuclear waste repositories (Berner et al., 2013; Claret et al., 2018; De Windt et al., 2007), environmental remediation (Jamieson-Hanes et al., 2012; Wanner et al., 2012; Wanner and Sonnenthal, 2013), etc.

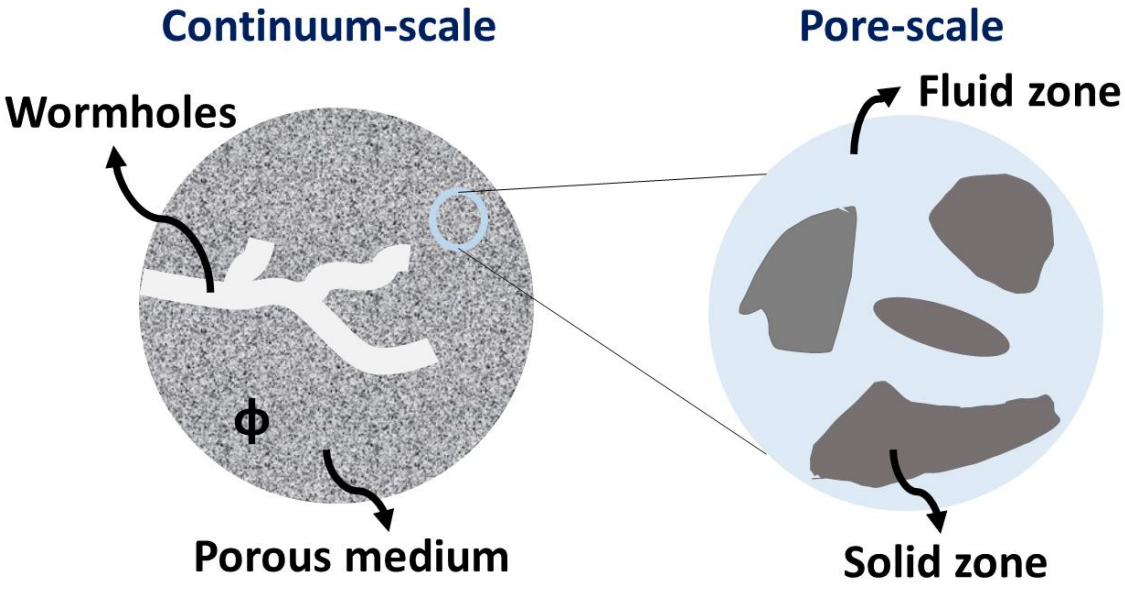

Figure 1: Schematic concept of continuum-scale and pore-scale approaches. In the continuum- or Darcy-scale approach, porosity ϕ ($0 < \phi < 1$) describes the porous medium. In pore-scale modelling, each control volume is determined by a specific phase, fluid or solid.

Three different kinds of models can be used to describe reactive transport in porous media: (1) continuum-scale models, (2) pore-scale models, and (3) hybrid-scale models that combine both continuum and pore-scale approaches. In the continuum- or Darcy-scale model, the porosity, which is a measure of void fraction with value ranging from 0 to 1, describes the porous medium. In pore–scale modelling, the medium is described by the volume fraction of pore which is the ratio of void space to the cell volume and the volume fraction of solid which is the ratio of solid zone to the cell volume (Figure 1).

1.1. BASIC GOVERNING EQUATIONS FOR A SINGLE-PHASE SINGLE COMPONENT FLUID

The governing equations, in the absence of electromagnetic effects, are the conservation of mass, linear momentum, angular momentum and energy (Truesdell and Noll, 1992). The conservation of mass in the Eulerian form is given by:

$$\frac{\partial \rho}{\partial t} + \boldsymbol{\nabla}\cdot(\rho \boldsymbol{v}) = 0 \tag{1}$$

where $\boldsymbol{v}$ is the velocity, ρ is the density, and $\partial/\partial t$ is the partial derivative with respect to time. The balance of linear momentum is

$$\rho \frac{d\boldsymbol{v}}{dt} = \nabla \cdot \boldsymbol{T} + \rho \boldsymbol{b} \tag{2}$$

where d/dt is the total time derivative, given by

$$\frac{d(.)}{dt} = \frac{\partial(.)}{\partial t} + [\boldsymbol{\nabla}(.)]\boldsymbol{v} \tag{3}$$

where **b** is the body force, and **T** is the Cauchy stress tensor. The balance of angular momentum (in the absence of couple stresses) yields the result that the Cauchy stress is symmetric. The energy equation in general can have the form (see Massoudi (2011):

$$\rho \frac{d\varepsilon}{dt} = \boldsymbol{T}.\boldsymbol{L} - \boldsymbol{\nabla}\cdot\boldsymbol{q} + \rho r + Q C_0 K_0 \tag{4}$$

where ε denotes the specific internal energy, **q** is the heat flux vector, r is the radiant heating, Q is the heat of reaction, C_0 is the initial concentration of the reactant species, K_0 is the reaction rate expression which is a function of temperature, and **L** is the velocity gradient. Thermodynamical considerations require the application of the second law of thermodynamics or the entropy inequality. The local form of the entropy inequality is given by (Liu, 2002) (p. 130):

$$\rho\dot{\eta} + \boldsymbol{\nabla}\cdot\boldsymbol{\varphi} - \rho s \geq 0 \tag{5}$$

where $\eta(x,t)$ is the specific entropy density, $\boldsymbol{\varphi}(x,t)$ is the entropy flux, and s is the entropy supply density due to external sources, and the dot denotes the material time derivative. If it is assumed that $\boldsymbol{\varphi} = \frac{1}{\theta}\boldsymbol{q}$, and $s = \frac{1}{\theta}r$, where θ is the absolute temperature, then Equation 5 reduces to the Clausius-Duhem inequality

$$\rho\dot{\eta} + \boldsymbol{\nabla}\cdot\left(\frac{q}{\theta}\right) - \rho\,\frac{r}{\theta} \geq 0 \tag{6}$$

For a complete thermo-mechanical study of a problem, the Second Law of Thermodynamics has to be considered (Liu, 2002; Müller, 1967; Truesdell and Noll, 1992; Ziegler, 1983).

Constitutive relations for complex materials can be obtained in different ways, for example, by using: (a) continuum mechanics, (b) physical and experimental models, (c) numerical simulations, (d) statistical mechanics approaches, and (e) ad-hoc approaches. A look at the governing Equation (1–4) reveals that constitutive relations are required for **T**, **q**, Q , ε, and r. In many practical problems involving competing effects such as temperature and concentration, the body force **b**, which in problems dealing with natural convection oftentimes depends on the temperature and can be modeled using the Boussinesq assumption (see Slattery (1999) in such a way that it is also a function of concentration.

Once appropriate constitutive relations are chosen and substituted in the above governing equations, a system of partial differential equations is obtained, which are then applied to a specific physical problem (a specific geometry with boundary and initial conditions) and then the equations are solved numerically. In most cases, advanced computational codes are necessary. In more complex situations such as multicomponent multiphase flows encountered in geological applications, where chemical reactions and heat transfer are to be considered, the above set of equations are no longer sufficient and instead one has to use the more advanced and more complicated multicomponent theories (see Bear and Bachmat (2012)).

2. CONTINUUM-SCALE MODELS

Porous medium has historically been treated as continuum to study flow, transport, and reactions in geological materials. In this approach, a representative volume (REV) is defined where at each point in space all phases are assumed to exist simultaneously. Bulk parameters such as porosity, permeability, or reactive surface area are then used to characterize the medium.

In the continuum-scale, Darcy's equation is usually used to model flow, and multicomponent species transport relies on a set of advection-dispersion-reaction equations. The limiting factor of the continuum-scale models is the determination of empirical parameters and their evolution as a function of the progress of geochemical processes, which often relies on constitutive relationships or equations such as Kozeny-Carman or Van Genuchten for permeability, Archie's law for tortuosity, or the two-third power law of porosity for mineral surface area (Xie et al., 2015).

Numbers of modern numerical reactive transport codes for subsurface simulations are based on continuum representations. These models include, but are not limited to, CrunchFlow (Steefel and Molins, 2009), STOMP (White and Oostrom, 1997, 2006), HYDROGEOCHEM (Yeh et al., 2004), OpenGeoSys (Kolditz et al., 2012), ORCHESTRA (Meeussen, 2003), PFlotran (Hammond et al., 2014; Lichtner et al., 2020a, 2020b), PHREEQC (Parkhurst and Appelo, 2013), TOUGHREACT (Xu et al., 2006; Xu et al., 2014), and MIN3P (Mayer et al., 2002). A few of these, including application examples, will be described below.

2.1. PFLOTRAN

PFLOTRAN is an open-source massively parallel subsurface flow and reactive transport code developed by Hammond and co-workers (Hammond et al., 2014; Lichtner et al., 2020a, 2020b). It is a multiple U.S. Department of Energy (DOE) laboratory effort with core developers from Los Alamos National Laboratory (LANL), Sandia National Laboratory (SNL), Laurence Berkeley National Laboratory (LBNL), and Oak Ridge National Laboratory (ORNL).

PFLOTRAN code solves a system of generally non-linear partial differential equations describing multiphase, multicomponent, and multiscale reactive flow and transport in porous materials. According to the authors, the current version of PFLOTRAN (version 4.0) can handle several subsurface processes involving flow and transport in porous media including Richards' equation, two-phase flow involving supercritical CO_2, and multicomponent reactive transport including aqueous complexing, sorption, and mineral precipitation and dissolution. Geochemical systems can be modeled in 1D, 2D, and 3D using structured or unstructured grids as discretization scheme. PFLOTRAN can solve the reactive transport equations with different finite difference methods (explicit, implicit, and operator-splitting). The code can handle multiple input files and multiple realizations simultaneously per run, which is useful for sensitivity analysis and uncertainty quantification. Some process models are under development including surface-subsurface flow coupling, geomechanics (elastic geomechanical model), and multiple continuum models for reactive transport.

The governing equations in the GENERAL mode, which involves two phase liquid water-gas flow coupled to the reactive transport mode, are as follows:

- Mass conservation equation

$$\frac{\partial}{\partial t}\phi\left(s_l\rho_l\chi_l^j + s_g\rho_g\chi_g^j\right) + \boldsymbol{\nabla}\cdot\left(\boldsymbol{V}_l\rho_l\chi_l^j + \boldsymbol{V}_g\rho_g\chi_g^j - \phi s_l D_l\rho_l\boldsymbol{\nabla}\chi_l^j - \phi s_g D_g\rho_g\boldsymbol{\nabla}\chi_g^j\right) = Q^j \quad (7)$$

where $s_{l,g}$, $\rho_{l,g}$, $D_{l,g}$, $\boldsymbol{V}_{l,g}$, $\chi_{l,g}^j$ are liquid and gas saturation, density, diffusivity, Darcy velocity and mole fraction of species j satisfying $\sum_j \chi_\gamma^j = 1$, respectively.

- Energy conservation equation

$$\sum_{\gamma=l,g}\left\{\frac{\partial}{\partial t}\left(\phi s_\gamma\rho_\gamma u_\gamma\right) + \boldsymbol{\nabla}\cdot\left(\boldsymbol{V}_\gamma\rho_\gamma h_\gamma\right)\right\} + \frac{\partial}{\partial t}\left((1-\phi)\rho_s c_s T\right) - \boldsymbol{\nabla}\cdot(\kappa\boldsymbol{\nabla}T) = Q^h \quad (8)$$

as the sum of contributions from liquid and gas fluid phases and rock, with internal energy u_γ and enthalpy h_γ of fluid phase γ, rock heat capacity c_s and thermal conductivity κ.

$$u_\gamma = h_\gamma - \frac{P_\gamma}{\rho_\gamma} \quad (9)$$

The Darcy velocity is given by $\boldsymbol{V}_\gamma = -\frac{kk_{r\gamma}}{\mu_\gamma}\boldsymbol{\nabla}\left(P_\gamma - \alpha_\gamma\boldsymbol{g}z\right)$, $(\gamma = l,\mathrm{g})$, where $\boldsymbol{g}$, k, $k_{r\gamma}$, μ_γ, and P_γ are the acceleration of gravity, saturated permeability, relative permeability, viscosity and pressure of the fluid phase γ, respectively. The quantity $\alpha_\gamma = W_\gamma\rho_\gamma$, with W_γ the gram formula weight of the phase γ.

h -enthalpy [kJ mol^{-1}]
k -intrinsic permeability [m^2]
k_r -relative permeability [-]
P -pressure [Pa]
$\boldsymbol{g}$ -gravity [m s^{-2}]
Q^j -source/sink [kmol m^{-3} s^{-1}]
V -Darcy flux [m s^{-1}]
s -saturation [m^3 m^{-3}]
T -temperature [K]
u -internal energy [kJ mol^{-1}]
W_γ -formula weight of phase γ [kg kmol^{-1}]
ϕ -porosity [-]
ρ -mass density [kg m^{-3}]
μ -viscosity [Pa s]
D -diffusivity [m^2 s^{-1}]

More information on the code can be found at https://www.pflotran.org/.

PFLOTRAN code has applications in many fields. For example, the code was used to model CO_2 injection and post-injection monitoring to evaluate long-term dissolution, leakage, footprint, and

pore pressure evolution in a storage system including a target aquifer, caprock, and an overlying aquifer (Zhang et al., 2017). Tutolo et al. (2015) utilized PFLOTRAN to investigate the coupled effects of cool CO_2 injection and background hydraulic head gradients on reservoir-scale mineral volume changes by examining the effects of temperature, pressure, hydraulic head gradient, and CO_2 injection rate on dissolution and precipitation processes in monomineralic calcite and dolomite CO_2 capture, utilization, and storage (CCUS) reservoirs. PFLOTRAN was also used to benchmark bench-scale supercritical CO_2-water mass transfer experiments into homogenous saturated porous media at pressures and temperatures relevant to geologic carbon sequestration (Newell et al., 2018). Navarre-Sitchler et al. (2013) explored changes to water chemistry in the event of a CO_2 leak into a shallow, heterogeneous, freshwater aquifer at a regional scale and relatively small-spatial resolution. Hypothetical aquifers were simulated to examine lead release and transport after CO_2 leakage. The code was also employed to assess the most relevant processes of metal release and attenuation at acid rock drainage (Mayer et al., 2015). Acid rock drainage is typically generated in mine waste deposits including tailings and waste rock piles, but also in abandoned mine workings (INAP, 2009; Nordstrom et al., 2000). Another area of application is the simulation of the fractionation of Cr isotope during aqueous kinetic Cr(VI) reduction (Wanner et al., 2015).

2.2. TOUGH AND TOUGHREACT

TOUGH ("**T**ransport **O**f **U**nsaturated **G**roundwater and **H**eat") is a suite of software codes developed at the LBNL. They are multi-dimensional numerical models for simulating the coupled transport of water, vapor, non-condensable gas, and heat in porous and fractured media (Pruess, 2004). The latest version of TOUGH codes is TOUGH3 which can be run in serial mode, on multi-processor machines, or massively-parallel clusters. TOUGHREACT was developed by introducing reactive chemistry into the multiphase flow code TOUGH2. TOUGHREACT can accommodate any number of chemical species present in liquid, gas, and solid phases. A variety of reactive processes are implemented such as aqueous and surface complexation, gas dissolution/exsolution, ion exchange, mineral dissolution/precipitation, and microbial mediated biodegradation. The temperature and pressure ranges are limited by the chemical thermodynamic database and the equation of state (EOS) module employed.

The primary governing equations for multiphase fluid and heat flow, and chemical transport have the same structure, derived from the principle of mass and energy conservation. Aqueous species are subject to transport in the liquid phase and local chemical interaction with the solid and gaseous phases. The transport equations are written in terms of total dissolved concentrations of chemical components, which are concentrations of the basis species plus their associated aqueous secondary species. Advection and diffusion are considered for chemical transport, and diffusion coefficients are assumed to be the same for all aqueous species.

General governing equations:

$$\frac{\partial \mathcal{M}^{\xi}}{\partial t} = -\nabla \boldsymbol{F}^{\xi} + Q^{\xi} \tag{10}$$

- Water:

$$\mathcal{M}^w = \phi\left(s_l\rho_l\omega_l^w + s_{\mathrm{g}}\rho_{\mathrm{g}}\omega_{\mathrm{g}}^w\right) \qquad \boldsymbol{F}^w = \omega_l^w\rho_l\boldsymbol{V}_l + \omega_{\mathrm{g}}^w\rho_{\mathrm{g}}\boldsymbol{V}_{\mathrm{g}} \qquad Q^w = Q_l^w + Q_{\mathrm{g}}^w \qquad (11)$$

- Air:

$$\mathcal{M}^a = \phi\left(s_l\rho_l\omega_l^a + s_{\mathrm{g}}\rho_{\mathrm{g}}\omega_{\mathrm{g}}^a\right) \qquad \boldsymbol{F}^a = \omega_l^a\rho_l\boldsymbol{V}_l + \omega_{\mathrm{g}}^a\rho_{\mathrm{g}}\boldsymbol{V}_{\mathrm{g}} \qquad Q^a = Q_l^a + Q_{\mathrm{g}}^a + Q_r^a \qquad (12)$$

- Heat:

$$\mathcal{M}^h = \phi\left(s_l\rho_l u_l + s_{\mathrm{g}}\rho_{\mathrm{g}}u_{\mathrm{g}}\right) + (1-\phi)\rho_s u_s \qquad \boldsymbol{F}^h = \sum_{\gamma=l,\mathrm{g}} h_\gamma\rho_\gamma\boldsymbol{V}_\gamma - \kappa\nabla T \qquad Q^h \qquad (13)$$

Where $\boldsymbol{V}_\gamma$ is the Darcy velocity,

$$\boldsymbol{V}_\gamma = -k\frac{k_{r\gamma}}{\mu_\gamma}\left(\nabla P_\gamma - \rho_\gamma\boldsymbol{g}\right) \qquad \gamma = l, \mathrm{g} \qquad (14)$$

Chemical components in the liquid phase (j = 1, 2 , … , N_1)

$$\mathcal{M}^j = \phi s_l C_l^j \qquad \boldsymbol{F}^j = \boldsymbol{V}_l C_l^j - (\tau\phi s_l D_l)\nabla C_l^j \qquad Q^j = Q_l^j + Q_{\mathrm{g}}^j + Q_s^j \qquad (15)$$

with $\tau_\gamma = \phi^{1/3}s_\gamma^{7/3}$

C component concentration [mol L^{-1}]
D diffusion coefficient [m^2 s^{-1}]
F mass flux [kg $m^{-2}s^{-1}$] (*)
k absolute permeability [m^2]
k_r relative permeability [-]
g gravitational acceleration [m s^{-2}]
M mass accumulation [kg m^{-3}]
N number of chemical components
P pressure [Pa]
Q source/sink
s saturation [-]
T temperature [^oC]
u internal energy [J kg^{-1}]
V Darcy velocity [m s^{-1}]
ω mass fraction [-]
ϕ porosity [-]
h enthalpy [J kg^{-1}]
τ medium tortuosity [-]

ρ density [kg m^{-3}]
μ viscosity [kg $m^{-1}s^{-1}$]
κ heat conductivity [W $m^{-1}K^{-1}$]

Subscripts:
a air
g gas phase
h heat
j aqueous chemical component
l liquid phase
r reaction
s solid phase
w water
ξ governing equation index
γ phase index

(*) For chemical transport and reaction calculations, molar units are used instead of kg.

Saturation s_γ is the fraction of pore volume occupied by phase γ.

The mass and energy balance equations are solved implicitly by Newton–Raphson iterations. Space discretization involves an unstructured finite volume scheme. TOUGHREACT uses EOS flow modules to compute fluid phase partitioning, and flow/transport of various components

(e.g., water, CO_2, salt, air, tracers, radionuclides) in liquid, gas, and nonaqueous phases. For example, if dealing with CO_2 (ECO2N), component "Air" above should be replaced with "CO_2". TOUGHREACT has also been coupled with a geomechanics simulator ROCMECH to study fractured geothermal reservoirs (Kim et al., 2015). More information can be found at https://tough.lbl.gov/.

TOUGHREACT has been applied in a variety of problems including mineral trapping for CO_2 disposal in deep saline aquifers (Xu et al., 2003a, 2004), modeling of mineral precipitation/dissolution in plug-flow and fracture-flow experiments under boiling conditions (Dobson et al., 2003), calcite precipitation in the vadose zone as a function of net infiltration (Xu et al., 2003b), coupled thermal, hydrological, and chemical processes in boiling unsaturated tuff for the proposed nuclear waste disposal site at Yucca Mountain, Nevada (Sonnenthal and Spycher, 2000; Spycher et al., 2003; Xu et al., 2001). The code has also been applied in isotope fractionation in unsaturated zone pore water and vapor (Singleton et al., 2004), mineral scaling during wastewater injection into a fractured geothermal reservoir (Xu et al., 2006), and CO_2 geological sequestration in a deep saline aquifer (Xu et al., 2006).

2.3. CRUNCHFLOW

CrunchFlow is a multicomponent reactive flow and transport code developed by Steefel and co-workers and applied since 1988 to a variety of problems in the earth and environmental sciences (Steefel et al., 2015; Steefel and Molins, 2009). It is based on a finite volume discretization of the governing coupled partial differential equations that link flow, solute transport, and multicomponent equilibrium and kinetic reactions in porous and/or fluid media. The features of the code include non-isothermal transport and reaction, and unsaturated transport with gas-aqueous phase exchange. A wide range of biogeochemical reactions are included in CrunchFlow, such as aqueous complexation, adsorption/desorption, ion-exchange, precipitation/dissolution, redox reactions, advection/diffusion, radiative decay chains, and microbial-mediated reactions. Two approaches are available for coupling reactions and transport, a global implicit approach that solves transport and reactions simultaneously, and a time or operator splitting approach based on the sequential non-iterative approach.

The reactive transport equations in CrunchFlow can be written as follows:

$$\frac{\partial(\phi\psi^j)}{\partial t} = \nabla\cdot(\phi\boldsymbol{D}\nabla\psi^j) - \nabla\cdot(\phi\mathbf{u}\psi^j) - \sum_m \nu_{j,m}R_m \qquad (j = 1, 2, \ldots, N_{tot}) \qquad (16)$$

The term on the left-hand side is the accumulation term, with the porosity, ϕ, multiplied by the total concentration (ψ^j) of each component j. The first, second, and third terms at the right-hand side represent the dispersion-diffusion, advection, and reaction terms, respectively. N_{tot} is the total number of components, $\mathbf{u}$ the flow velocity (m/s), and $\boldsymbol{D}$ the dispersion-diffusion tensor (m^2/s). The total concentration of component j is the summation of the concentration of primary species j, and the contributions of all secondary species k, weighted by the stoichiometric coefficient $\nu_{k,j}$ as follows:

$$\psi^j = C^j + \sum_k \nu_{k,j} C^k \tag{17}$$

The concentration of the secondary species C_j (mol/m^3) is calculated from the concentrations of primary species based on aqueous complexation reactions, which are assumed to be at equilibrium,

$$C^k = \gamma_k^{-1} K_{eq,k}^{-1} \prod_j \left(\gamma_j C^j\right)^{\nu_{k,j}} \tag{18}$$

where K_{eq} is the equilibrium constant, and γ_j is the activity coefficient that is calculated using the extended Debye-Hückle equation. ϕ is the porosity [m^3 void m^{-3} medium] and R_m rate of reaction (mol/m^3/s)

In the application fields, CrunchFlow was used to simulate the infiltration of hyperalkaline groundwater along discrete fractures at Maqarin, Jordan, a proposed natural analogue site to cement bearing nuclear waste repositories (Steefel and Lichtner, 1998). CrunchFlow was also employed to study heavy metal cycling in mining-impacted lake sediments (Arora et al., 2015), to assess the most relevant processes of metal release and attenuation at acid rock drainage (Mayer et al., 2015), and to simulate the fractionation of Cr isotope during aqueous kinetic Cr(VI) reduction (Wanner et al., 2015). Bagheri et al. (2019) coupled CrunchFlow with a geomechanical model to predict the lifespan of a cement matrix exposed to CO_2-bearing fluids at a specific depth at the conditions found in depleted oil and gas reservoirs.

Table 1: Summary of Key Capabilities of Selected Continuum-Scale Model Reactive Transport Codes. A more detailed description of the capabilities of the codes can be found in Steefel et al. (2015).

Continuum-Scale Models	Flow and Heat Transfer	Mass Transfer	Biogeochemistry	Geo-mechanics
OpenGeoSys	Saturated Variable density Two-phase Non-isothermal	Diffusion Advection Multicomponent Multiple continua Colloids	Complexation Adsorption-Desorption Precipitation-Dissolution Ion exchange Nucleation Isotope fractionation	Elastic and inelastic deformations
STOMP	Saturated Variable density Multiphase Non-isothermal	Diffusion Advection Multicomponent	Complexation Precipitation-Dissolution Ion exchange Nucleation	Thermo-poro-elastic + small strain assumption
PFLOTRAN	Saturated Constant density Multiphase Non-isothermal	Diffusion Advection Multicomponent-multispecies Multiple continua Colloids	Complexation Adsorption-Desorption Precipitation-Dissolution Ion exchange	Under development Linear elastic deformation
TOUGHREACT	Saturated Multiphase Variable density Non-isothermal	Diffusion Advection Multicomponent-multispecies Multiple continua Colloids	Complexation Adsorption-Desorption Precipitation-Dissolution Ion exchange Isotope fractionation	Pore compressibility
Crunchflow	Saturated Variable density Single phase	Diffusion Advection Electrochemical migration Multiple continua	Complexation Ion exchange Precipitation-Dissolution Nucleation Isotope fractionation	Unavailable
MIN3P	Saturated Unsaturated Variable density Single phase Non-isothermal	Diffusion Advection Multicomponent-multispecies Electrochemical migration Multiple continua	Complexation Adsorption-Desorption Precipitation-Dissolution Ion exchange Isotope fractionation	1D vertical stress

2.4. MIN3P / MIN3P-HPC

MIN3P is a general-purpose multicomponent flow and reactive transport code for variably saturated media, which provides a high degree of flexibility with respect to the definition of the reaction network (Mayer et al., 2002). The key features of the MIN3P code include 3D saturated/unsaturated fluid flow, biogeochemical reactions, heat transport, solute and gas transport, density coupling between flow and transport, and 1D hydromechanical coupling (Bea et al., 2016; Bea et al., 2012; Henderson et al., 2009; Mayer et al., 2002; Mayer and MacQuarrie, 2010; Su et al., 2017). Several code developments have been performed since the release of the original version in 1999. Code capabilities were enhanced with the inclusion of: the dual porosity model (MIN3P-DUAL) by Cheng (2005), and used to assess the fate and transport of methyl tertiary butyl ether (MTBE) in a Chalk aquifer (Cheng et al., 2011); gas exsolution, entrapment and release model (MIN3P-BUBBLE) by Amos and Mayer (2006a,b); multicomponent gas phase diffusion and advection model (MIN3P-DUSTY) to simulate gas attenuation in partially saturated landfill soil covers, methane production, and oxidation in aquifers contaminated by organic compounds and pyrite oxidation in mine tailings (Molins et al., 2008; Molins and Mayer, 2007); and density coupling between flow and reactive transport (MIN3P-D) by Henderson et al. (2009). MIN3P capabilities were further enhanced with the implementation of the Pitzer equations for activity corrections, energy balance, and a formulation for 1D vertical stress (MIN3P-THCm, Bea et al., 2011, 2012); and the latest release of the high-performance unstructured grid code (MIN3P-HPC) for subsurface flow and reactive transport simulation (Sue et al., 2021).

The main governing equations in MIN3P-HPC are summarized below.

a) The flow equation is that of a non-isothermal and density-dependent variably saturated flow and described as following (Bea et al., 2012; Henderson et al., 2009):

$$\phi s_l \frac{\partial \rho_l}{\partial t} + \rho_l \frac{S_s}{\rho_w g}\left(\frac{\partial P}{\partial t} - \xi \frac{\partial \sigma_{zz}}{\partial t}\right) = -\nabla \cdot \rho_l \boldsymbol{V}_l + Q_l \tag{19}$$

where ϕ [L^3 void L^{-3} bulk] is porosity, s_l [L^3 water L^{-3} void] is the saturation of the aqueous phase and ρ_l [M L^{-3}] is the pore water density, which is a function of temperature and solution composition. ρ_w [M L^{-3}] is the freshwater density, t [T] is time, P [M L^{-1} T^{-2}] is the fluid pressure, S_s [L^{-1}] is the 1D specific storage coefficient, g [L T^{-2}] is the gravity constant, ξ [–] is a 1D loading efficiency coefficient, σ_{zz} [M L^{-1} T^{-2}] is the vertical component of the mean total stress and Q_l [M L^{-3} T^{-1}] is a source-sink term for the aqueous phase. The aqueous phase flux $\boldsymbol{V}_l$ [L T^{-1}] can be defined as

$$\boldsymbol{V}_l = -\frac{k_{rl}\boldsymbol{k}}{\mu}(\nabla P + \rho_l g \nabla z) \tag{20}$$

where k_{rl} [–] is relative permeability, $\boldsymbol{k}$ [L^2] is the permeability tensor and μ [M L^{-1} T^{-1}] is the dynamic fluid viscosity.

b) The energy transport is written according to the energy balance equation as follows

$$\frac{\partial \phi c_l s_l \rho_l}{\partial t} + \frac{\partial \phi c_g s_g \rho_g}{\partial t} + \frac{\partial (1-\phi) c_s \rho_s}{\partial t} + \frac{\partial L_w \phi s_g \rho_g}{\partial t} = \nabla \cdot \mathrm{J}^h + Q^h \tag{21}$$

where c_l, c_g, and c_s [E M^{-1} °C^{-1}] are the heat capacities for aqueous, gas (vapor) and solid phases, respectively; ρ_g, and ρ_s [M L^{-3}] are the density of gas (vapor) and solid phase, respectively; s_g [L^3 gas L^{-3} void] is the gas (vapor) phase saturation; $\nabla \cdot \mathrm{J}^h$ [E L^{-3} T^{-1}] is the energy flux; L_w [E M^{-1}] is the water vaporization latent heat; and Q^h [E L^{-3} T^{-1}] is an energy source-sink term.

c) The reactive transport equations are given by the global mass conservation equations for reactive transport in variably saturated porous media, with contributions from all mobile, adsorbed, and mineral species (Mayer et al., 2002)

$$\frac{\partial}{\partial t}\left[s_l \phi \psi_l^j\right] + \frac{\partial}{\partial t}\left[s_g \phi \psi_g^j\right] + \frac{\partial \psi_s^j}{\partial t} + \nabla \cdot \left[\boldsymbol{V}_l \psi_l^j\right] - \nabla \cdot \left[s_l \phi \boldsymbol{D}_l \nabla \psi_l^j\right] - \nabla \cdot \left[s_g \phi \boldsymbol{D}_g \nabla \psi_g^j\right] - Q^j = 0$$
$$j = 1, \ldots, N_c \; ; \tag{22}$$

where N_c is the number of components; ψ_l^j [M L^{-3}] and ψ_g^j [M L^{-3}] are the total aqueous component concentration and gaseous concentration for the component j, respectively; ψ_s^j [M L^{-3}] is the total concentration of aqueous component j on the surface sites; $\boldsymbol{D}_l$ [L^2 T^{-1}] is the dispersion tensor for the aqueous phase; $\boldsymbol{D}_g$ [L^2 T^{-1}] is the diffusion tensor for the gaseous phase; Q^j [M L^{-3} T^{-1}] is a summation of internal source and sink terms from intra-aqueous kinetic reactions and kinetically controlled dissolution-precipitation reactions, and external source and sink terms for the aqueous phase and gas phase. More information can be found at https://www.min3p.com/.

MIN3P has been applied in mining (Mayer et al., 2015; Vriens et al., 2020), deep geologic repositories (Su et al., 2018; Xie et al., 2014), oil and gas (Forde et al., 2018; Hers et al., 2014), carbon sequestration (Bea et al., 2012; Harrison et al., 2015), soil and plants (De Biase et al., 2012; Jia et al., 2021), and permeable reactive barriers (Bilardi et al., 2013; Mayer et al., 2006). For example, the code was used to model the generation and attenuation of acid drainage (Mayer et al., 2015), investigate the scale dependence of effective geochemical rates in weathering mine waste rock (Vriens et al., 2020). Hers et al. (2014) used MIN3P to assess the influence of winter conditions including snow/frost cover, and cold soil temperatures, on the aerobic biodegradation of petroleum vapors in soil and the potential for vapor intrusion. De Biase et al. (2012) simulated the removal of volatile organic compound in vertical flow soil filters and Jia et al. (2021) modelled the degradation of soil organic matter under variably saturated flow conditions.

2.5. OPENGEOSYS

OpenGeoSys (OGS) is a scientific open-source project for the development of numerical methods for the simulation of thermo-hydro-mechanical-chemical (THMC) processes in porous and fractured media. It is a finite element code based on an object-oriented and process-oriented approach that allows the solution of partial differential equations for different physical subsurface problems using a generic object structure (Kolditz and Bauer, 2004; Kolditz et al., 2012a; Wang and Kolditz, 2007). Fluid flow can be solved in a pressure-pressure or in a pressure-saturation formulation. Coupled processes are solved either sequentially (iterative and explicit coupling) or monolithically (fully coupled). For the geomechanical process, several constitutive models are implemented. The poroelastic model uses Biot formulation to solve for solid displacements, stresses, and strains.

The mathematical framework or governing equations to be solved when dealing with THMC processes in porous media can be described as follow (Kolditz et al., 2012a):

- For the heat transport (T process - thermodynamics) in multiphase systems, which includes phase changes such as evaporation, condensation and latent heat, the equation is given by

$$c\rho\frac{\partial T}{\partial t} = -\nabla\left(-\kappa\nabla T + \sum_{\gamma} h_{\gamma}\boldsymbol{F}_{\gamma}\right) + Q \tag{23}$$

where c is the heat capacity (J/kg K), ρ the density (kg/m^3), κ thermal conductivity (J/K m s), h_{γ} enthalpy of phase γ (J/kg), and T the temperature (K).

- The fluid flow (H process - hydraulics) is given by the equations of the non-isothermal multiphase flow of liquids and gases

$$\frac{\partial \mathcal{M}^{\xi}}{\partial t} = -\nabla\boldsymbol{F}^{\xi} + Q^{\xi} \tag{24}$$

$$\mathcal{M}^{\xi} = \phi\sum_{\gamma}\rho_{\gamma}s_{\gamma}\omega_{\gamma}^{\xi} \tag{25}$$

$$\boldsymbol{F}_{\gamma}^{\xi} = -\rho_{\gamma}\frac{\boldsymbol{k}k_{r\gamma}}{\mu_{\gamma}}\left(\nabla P_{\gamma} - \rho_{\gamma}\boldsymbol{g}\right), \quad \sum_{\gamma} s_{\gamma} = 1 \tag{26}$$

where ω_{γ}^{ξ} is the mass fraction of component ξ in phase γ, and ρ_{γ} phase density of phase γ (kg/m^3).

- The mass transport (C process - chemistry) equations for multicomponent including bio/geochemical reactions are obtained using the following expressions

$$\boldsymbol{F}^{\xi} = \sum_{\gamma} \left(\omega_{\gamma}^{\xi} \boldsymbol{F}_{\gamma} + \rho_{\gamma} \boldsymbol{D}_{\gamma}^{\xi} \nabla \omega_{\gamma}^{\xi} \right) \tag{27}$$

$$\ln\left(K_{P,T}\right) = \frac{\Delta G_{P,T}^{0}}{RT} \tag{28}$$

$$K_j = \frac{a_w^{\nu_{wj}} \prod_i \left(\gamma_i C^i\right)^{\nu_{ij}} \prod_m (a_m)^{\nu_{mj}} \prod_g \left(f_g\right)^{\nu_{gj}}}{\gamma_j C^j} \tag{29}$$

where $\boldsymbol{D}_{\gamma}^{\xi}$ is the diffusion tensor of component ξ for phase γ (m^2/s), $\Delta G_{P,T}^{0}$ standard Gibbs free energy (J/mol), R gas constant (J/mol K), and $K_{P,T}$ equilibrium constant at temperature T and pressure P.

- For deformations (M process - mechanics) non-isothermal elastic and inelastic deformations are considered according to the following equations

$$\nabla \boldsymbol{\sigma} - \rho \boldsymbol{g} = 0 \tag{30}$$

$$\nabla \cdot \left(\boldsymbol{\sigma} - \left(s_l P_l + s_{\mathrm{g}} P_{\mathrm{g}} \right) \mathbf{I} - \beta_T \Delta T \mathbf{I} \right) + \rho \boldsymbol{g} = 0 \tag{31}$$

where $\boldsymbol{\sigma}$ is the stress tensor (Pa), β_T the thermal expansion coefficient (K^{-1}), and $\mathbf{I}$ the identity tensor.

The equilibrium constant K_j at the temperature and pressure of interest is obtained through the law of mass action approach applied to a system with a basis (A_w, A_i, A_m, A_{g}), where A_w is water, A_i are the aqueous species, A_m the minerals, and A_g the gases in the basis. Secondary species can be expressed by the formation reactions of base species as the following reaction

$$A_j \rightleftharpoons \nu_{wj} A_w + \sum_i \nu_{ij} A_i + \sum_m \nu_{mj} A_m + \sum_{\mathrm{g}} \nu_{\mathrm{g}j} A_{\mathrm{g}} \tag{32}$$

where ν represents the reaction coefficients: ν_{wj} is the number of moles of water in the reaction to form A_j, ν_{ij} is the number of moles of the basis species A_i, and so on for the minerals and gases. γ_i and γ_j are the activity coefficients for the primary and secondary species, respectively; C^i and C^j the concentration of the primary and secondaries species, respectively; and a_i and f_{g} the activity of the species and fugacity of the gases, respectively. More information about the code can be found at https://www.opengeosys.org/.

The OGS community has been very active in several international benchmarking initiatives that has led to the publication of a book series containing well verified benchmarks (Kolditz et al.,

2012b; Kolditz et al., 2016; Kolditz et al., 2018; Kolditz et al., 2015). The versality of OGS platform has promoted functionality extension through code coupling interfaces to other simulators such as the reservoir simulator suite Eclipse (Graupner et al., 2011), the geochemical modeling package GEM (Shao et al., 2009; Shao et al., 2009), the Biogeochemical Reaction Network Simulator BRNS (Centler et al., 2010), the thermodynamic simulator ChemApp (Xie et al., 2011).

Current applications of OGS are CO_2 storage and sequestration (Benisch et al., 2013; Beyer et al., 2012; Böttcher et al., 2012; Singh et al., 2014), geothermal energy (Beyer et al., 2016; Pfeiffer et al., 2016), water resources management (Beyer et al., 2016), hydrology and waste deposition (Goerke et al., 2011; Shao et al., 2009). For example, OGS was coupled to the geochemical model ChemApp to assess the impact of geochemical reactions during CO_2 sequestration at a hypothetical but typical Bunter sandstone formation in the Northern German Basin (Li et al., 2014). OGS was applied to simulate the clogging process at Maqarin natural analogue site in Jordan (Shao et al., 2013). The code was also applied to predict heat transport processes due to a high-temperature heat injection, as well as the induced thermal impacts of a high temperature-aquifer thermal energy storage system (Heldt et al., 2021). OGS was used to study organic carbon degradation in a sand column via multiple microbial degradation pathways, and a dispersive mixing controlled bioreactive transport problem in aquifers with different reaction kinetics (Center et al., 2010). OGS was also coupled with PHREEQC to simulate geochemical processes such as ion exchange, mineral dissolution/precipitation, and equilibrium reactions in partly saturated bentonites (Xie et al., 2006). OpenGeoSys-Eclipse was used to address the impact of pore pressure changes on rock stability and deformation as well as the feedback effects of geomechanical processes on multiphase flow via pore volume coupling and porosity and permeability update (Benisch et al., 2020).

2.6. STOMP

Subsurface Transport Over Multiple Phases (STOMP) is a suite of numerical simulators developed by the Pacific Northwest National Lab (PNNL) for investigating coupled processes involving multifluid flow, heat transport, geochemistry, and geomechanics in the subsurface (Ward et al., 2012). It is designed to solve a wide variety of non-linear, multiple-phase, flow, and transport problems for variably saturated geologic media.

STOMP simulator is comprised of Operational Modes classified according to the solved governing flow and transport equations and constitutive relation extensions. The following Operational Modes are available in the STOMP simulator: STOMP-W for variably saturated flow and transport in water systems, STOMP-GT for geothermal systems, STOMP-CO2 for carbon storage applications, STOMP-EOR for enhanced oil recovery applications, STOMP-HYDT-KE for gas hydrates, STOMP-WO for non-volatile Organic, and STOMP-WOA for volatile Organic.

The governing equations that describe flow and transport through porous media in the STOMP simulator are conservation equations for component mass, energy, and solute (White and Oostrom, 2000). The components are referred here by water, air, oil, salt, and surfactants terms. The phases are referred by aqueous, gas, hydrate, non-aqueous phase liquid (NAPL), and solid. The component conservation equation defined as the time rate of change of component within a control volume with the flux of component crossing the control volume surface can be written in general form as follows

$$\frac{\partial \mathcal{M}^{\xi}}{\partial t} = -\nabla \boldsymbol{F}^{\xi} + Q^{\xi} \tag{33}$$

where $\mathcal{M}^{\xi}$ is the mass or heat accumulation, $\boldsymbol{F}^{\xi}$ the mass or heat flux and Q^{ξ} the sink and source terms.

- Water mass conservation

$$\mathcal{M}^{w} = \sum_{\gamma=l,\mathrm{g},ic} \left(\phi_D \omega_{\gamma}^{w} \rho_{\gamma} s_{\gamma}\right) \qquad \boldsymbol{F}^{w} = \sum_{\gamma=l,\mathrm{g}} \left(\boldsymbol{F}_{\gamma}^{w} + \boldsymbol{J}_{\gamma}^{w}\right) + \boldsymbol{F}_{l}^{S} \qquad Q^{w} = \dot{m}^{w} \tag{34}$$

- Air mass conservation

$$\mathcal{M}^{a} = \sum_{\gamma=l,\mathrm{g}} \left(\phi_D \omega_{\gamma}^{a} \rho_{\gamma} s_{\gamma}\right) \qquad \boldsymbol{F}^{a} = \sum_{\gamma=l,g} \left(\boldsymbol{F}_{\gamma}^{a} + \boldsymbol{J}_{\gamma}^{a}\right) \qquad Q^{a} = \dot{m}^{a} \tag{35}$$

- Oil mass conservation

$$\mathcal{M}^{o} = \sum_{\gamma=l,\mathrm{g},n} \left(\phi_D \omega_{\gamma}^{o} \rho_{\gamma} s_{\gamma}\right) + (1-\phi_T)\omega_{s}^{o}\rho_{s} \quad \boldsymbol{F}^{o} = \sum_{\gamma=l,\mathrm{g},n} \left(\boldsymbol{F}_{\gamma}^{o} + \boldsymbol{J}_{\gamma}^{o}\right) \quad Q^{o} = \dot{m}^{o} \tag{36}$$

- Energy Conservation

$$\mathcal{M}^{h} = \sum_{\gamma=l,\mathrm{g},n,ic} \left(\phi_D \rho_{\gamma} s_{\gamma} u_{\gamma}\right) + (1-\phi_T)\rho_{s} u_{s} + (\phi_T - \phi_D)\rho_{l} u_{l} \tag{37}$$

$$\boldsymbol{F}^{h} = \sum_{\gamma=l,\mathrm{g},n} \left(\rho_{\gamma} h_{\gamma} \mathbf{V}_{\gamma} + \sum_{j=w,a,o} h^{j} \boldsymbol{J}_{\gamma}^{j} \right) + \boldsymbol{\kappa}_{e} \nabla T \qquad Q^{h} = \sum_{j=w,a,o} \left(h^{j} \dot{m}^{j}\right) + \dot{q} \tag{38}$$

- Salt and surfactant mass conservation

$$\mathcal{M}^{S} = S \qquad \boldsymbol{F}^{S} = S_{l}\mathbf{V}_{l} - \left(\boldsymbol{\tau}_{l} s_{l} \phi_D D_{l}^{S} + s_{l}\phi_D \boldsymbol{D}_{h_l}\right)\nabla S_{l} \qquad Q^{S} = \dot{m}^{S} \tag{39}$$

- Solute mass conservation

$$\mathcal{M}^{C} = C \;\; \boldsymbol{F}^{C} = \sum_{\gamma=l,\mathrm{g},n} \left(C_{\gamma}\mathbf{V}_{\gamma}\right) - \sum_{\gamma=l,\mathrm{g},n} \left(\boldsymbol{\tau}_{\gamma} s_{\gamma} \phi_D D_{\gamma}^{C} + s_{\gamma}\phi_D \boldsymbol{D}_{h_\gamma}\right)\nabla C_{\gamma} \;\; Q^{C} = \dot{m}^{C} - \dot{R}^{C} C \tag{40}$$

where

$$\boldsymbol{F}_{\gamma}^{j} = -\frac{\omega_{\gamma}^{j}\rho_{\gamma}k_{r\gamma}\boldsymbol{k}}{\mu_{\gamma}}\left(\nabla P_{\gamma} + \rho_{\gamma}g\boldsymbol{z}_{g}\right) \quad for\ \gamma = l,\mathrm{g},n\ ;\ \ j = w,a,o \tag{41}$$

$$\boldsymbol{J}_{\gamma}^{j} = -\boldsymbol{\tau}_{\gamma}\phi_{D}\rho_{\gamma}s_{\gamma}\frac{M^{j}}{M_{\gamma}}D_{\gamma}^{j}\nabla\chi_{\gamma}^{j} \qquad for\ \gamma = l,\mathrm{g},n\ ;\ \ j = w,a,o \tag{42}$$

$$\boldsymbol{F}_{l}^{S} = D_{l}^{S}\nabla S_{l} \tag{43}$$

$$\mathbf{V}_{\gamma} = -\frac{k_{r\gamma}\boldsymbol{k}}{\mu_{\gamma}}\left(\nabla P_{\gamma} + \rho_{\gamma}g\boldsymbol{z}_{g}\right) \qquad for\ \gamma = l,\mathrm{g},n \tag{44}$$

The subscripts g, ic, l, n, and s are for gas phase, ice phase, aqueous phase, NAPL phase, and rock/soil or solid phase, respectively. The superscripts a, o, and w are for air, oil, and water components, respectively.

C and C_{γ} are the solute concentration and solute concentration in phase γ (1/m^3), respectively; D_{γ}^{j}, D_{γ}^{C}, and D_{γ}^{S} are the diffusion coefficient of component j, solute diffusion coefficient and salt diffusion coefficient for phase γ (m^2/s), respectively. $\boldsymbol{D}_{h_{\gamma}}$ is hydraulic dispersion tensor for phase γ (m^2/s). $\boldsymbol{F}_{l}^{S}$ and $\boldsymbol{F}_{\gamma}^{j}$ are the osmotic flux of the aqueous phase and the advective flux of component j in phase γ (kg/m^2 s), respectively. h^{j} and h_{γ} are the enthalpy of component j and the enthalpy of phase γ (J/kg), respectively. $\boldsymbol{J}_{\gamma}^{j}$ is the diffusive-dispersive flux of component j for the γ phase (kg/m^2 s); $k_{r\gamma}$ fluid relative permeability of phase γ; $\boldsymbol{k}$ intrinsic permeability tensor (m^2); $\boldsymbol{k}_{e}$ equivalent thermal conductivity tensor (W/m K). The quantities $\dot{m}^{j}$, $\dot{m}^{C}$, and $\dot{m}^{S}$ determine the mass source rate of component j (kg/s), solute rate (1/s), and the salt mass source rate (kg/s), respectively. M^{j} and M_{γ} are the molecular weight of component j and phase γ (kg/kgmol), respectively. Other quantities are: $\dot{q}$ thermal energy source (W), $\dot{R}^{C}$ solute decay rate constant (1/s), S salt concentration (kg/m^3), S_{l} salt concentration in phase γ (kg/m^3), s_{γ} saturation of phase γ, u_{γ} internal energy of phase γ (J/kg), u_{s} porous media internal energy (J/kg), $\mathbf{V}_{\gamma}$ Darcy velocity vector of phase γ (m/s), μ_{γ} kinematic viscosity of phase γ (Pa s), ρ_{γ} phase density for phase γ (kg/m^3), $\boldsymbol{\tau}_{\gamma}$ phase tortuosity for phase γ, χ_{γ}^{j} mole fraction of component j in phase γ, and ω_{γ}^{j} mass fraction of component j in phase γ.

The partial-differential equations describing the conservation of mass and energy are solved using finite volume method for spatial discretization and backward Euler method for time discretization. An operator splitting solution method is used for flow, transport, and reactions, each of which employs implicit time-stepping schemes. The resulting non-linear coupled algebraic equations are solved using Newton–Raphson iteration. Reactive transport is implemented through the ECKEChem module (White and McGrail, 2005). The implementation

of the geomechanical model through the GeoMech module gives the STOMP simulator fully coupled THMC capabilities. Reactive processes considered include aqueous and surface complexation, ion exchange, mineral precipitation-dissolution, and aqueous-gas exchange. Microbially mediated reactions include species-specific biomass production and decay, Monod-type rate laws with biomass dependencies, and thermodynamic controls. Transport algorithms address advection, anisotropic dispersion, and interphase partitioning. More information can be found at https://www.pnnl.gov/projects/stomp.

STOMP has a vast field of applications including geologic sequestration (e.g., deep sedimentary saline formations (Nguyen et al., 2016), enhanced oil recovery (Bacon et al., 2015; White et al., 2014), environmental remediation (e.g., non-aqueous phase liquid and dense NAPL fate, transport, and remediation (Matos de Souza et al., 2016; Yoon et al., 2009); soil desiccation (Oostrom et al., 2012), environmental stewardship (e.g., radionuclide and contaminant fate and transport (Oostrom et al., 2007), storage tank leaks (Bacon et al., 2016), unconventional hydrocarbon and energy development (e.g., methane gas hydrate production (Ju et al., 2020; White et al., 2011), and natural gas (White et al., 2020).

3. PORE-SCALE MODELS

Pore-scale is defined as the scale at which each point of space in the pore network is occupied by a specific phase, fluid or solid. Contrary to the continuum-scale, pore-scale modeling requires an exact knowledge of the phase distribution. Reactive transport at the pore-scale is still emerging. One of the main challenges of the pore-scale approach is the characterization of the solid/fluid interfaces and the evolution of the interfaces with respect to chemical reactions at the mineral boundaries (Molins et al., 2021; Noiriel and Soulaine, 2021).

Popular approaches to pore-scale modeling applied to reactive geochemical systems include the Lattice Boltzmann method (LBM), Lagrangian approach and particle methods, and computational fluid dynamics (CFD).

3.1. THE LATTICE BOLTZMAN METHOD

The LBM has made significant progress in modeling fluid flow in porous media and reactive transport. It was developed as an extension to lattice gas models (LGMs) for fluid flows. In a LGM, particles move synchronously from node to node on a regular Bravais lattice and undergo momentum-conserving collisions (d'Humières et al., 1986; Frisch et al., 1986). However, LGMs suffer from major deficiencies for use in hydrodynamic simulations such as lack of Galilean invariance for fast flows, statistical noise, and poor Reynolds number scaling with lattice size. To overcome these deficiencies the LBM uses a mesoscale approach in which the amount of fluid associated with each lattice node is large enough to suppress the effects of fluctuations through averaging. In one approach, Higuera and Jimenez (1989) replaced the discrete collision by a linearized collision operator by assuming that the distribution is close to the local equilibrium state. The Bhatnagar-Gross-Krook (BGK) relaxation term (Bhatnagar et al., 1954) is the simplest and most used to approximate the linearized collision operator, making simulations more efficient and allowing flexibility of the transport coefficients. From Chapman-Enskog theory, one can recover the governing continuity and Navier–Stokes equations (in an incompressible limit) from the LBM algorithm (Wolf-Gladrow, 2000). LBM presents several advantages, and it can easily deal with complex boundaries using a simple bounce-back or modified bounce-back scheme (He and Luo, 1997) in the fluid particle distributions. It can be applied to multiphase flow with phase transition and particulate suspension flows. One of the limitations of LBM is that flows with Mach numbers greater than 0.1 and flows with pressure variations or density variations greater than 0.01 will exhibit significant deviations from incompressible Navier-Stokes flows. The method has been successfully applied to model flow and reactive transport phenomena in a various media.

For example, Kang et al. (2006, 2007) developed a multicomponent pore-scale LBM model to simulate reactive transport with both homogeneous and heterogeneous reactions between the multiple aqueous species and minerals. They further applied the model in CO_2 geologic sequestration to simulate the injection of CO_2-saturated brine into structured porous media (Kang et al., 2010). Tian et al. (2016) developed a geochemical reaction LBM model at the representative elementary volume-scale to investigate the coupled processes of fluid flow, solid phase dissolution, and species reactive transport in homogeneous porous media. The change in porosity due to dissolution and its impacts on flow field were numerically analyzed. The model was then extended to study the reactive transport of CO_2 injection in fractured reservoirs (Tian et al., 2016). LBM models have also been used for applications in nuclear waste repositories (Curti

et al., 2019; Prasianakis et al., 2017) and multiphase reacting flow in magma chambers (Huber et al., 2014; Parmigiani et al., 2011).

Below is a brief description of an LBM model.

The generalized Navier-Stokes equations for isothermal incompressible fluid flow through porous media are:

$$\rho \frac{\partial \mathbf{u}}{\partial t} + \rho \mathbf{u} \cdot \nabla \mathbf{u} = -\nabla P + \mu \nabla^2 \mathbf{u} \tag{45}$$

$$\nabla \cdot \mathbf{u} = 0 \tag{46}$$

where ρ and μ are the fluid density and the effective viscosity, respectively.

In the LBM framework the motion of fluid can be described by a set of particle distribution functions. Based on the simple and popular BGK collision operator, the evolution equation of the particle distribution function f_i is as follows:

$$f_i(\mathbf{x} + \boldsymbol{v}_i \Delta t, t + \Delta t) - f_i(\mathbf{x}, t) = -\frac{1}{\zeta}\left[f_i(\mathbf{x}, t) - f_i^{eq}(\mathbf{x}, t)\right] \tag{47}$$

The terms **x** and t represent the node position and time, $\boldsymbol{v}_i$ the particle discrete velocity along the *i*th discrete direction; Δt and ζ are the time step and the dimensionless relaxation time, respectively, and f_i^{eq} is the equilibrium distribution function. The fluid density and velocity are defined as:

$$\rho = \sum_i f_i \ , \quad \rho \mathbf{u} = \sum_i \boldsymbol{v}_i f_i \tag{48}$$

Using the Chapman–Enskog procedure, the above generalized N–S equation can be recovered in the incompressible limit.

The transport of aqueous species in the LBM can also be described by an evolution distribution:

$$g_{\alpha,i}(\mathbf{x} + \boldsymbol{v}_i \Delta t, t + \Delta t) - g_{\alpha,i}(\mathbf{x}, t) = -\frac{1}{\zeta_\alpha}\left[g_{\alpha,i}(\mathbf{x}, t) - g_{\alpha,i}^{eq}(\mathbf{x}, t)\right] \tag{49}$$

where $g_{\alpha,i}$ is the concentration distribution function for the αth species, ζ_α is the dimensionless relaxation time for the αth species, and $g_{\alpha,i}^{eq}$ is the equilibrium distribution function for the αth species. The species or solute concentration is obtained by

$$C^\alpha = \sum_i g_{\alpha,i} \tag{50}$$

and the diffusivity is related to the relaxation time. One can recover the following pore-scale advection-diffusion equation for C^α:

$$\frac{\partial C^\alpha}{\partial t} + (\mathbf{u} \cdot \nabla) C^\alpha = \nabla \cdot (D \nabla C^\alpha). \tag{51}$$

The quantity D is the diffusion coefficient. More details can be found in Kang et al. (2010, 2006, 2007), Chen et al. (2015) and Tian et al. (2016).

3.2. LAGRANGIAN APPROACH AND PARTICLE METHODS

A variety of particle methods have been developed for the purpose of modelling and simulating single- and multi-phase fluid flow and reactive transport in fractured and porous media (Meakin and Tartakovsky, 2009). Examples of these methods include dissipative particle dynamics (Drawert et al., 2019), vortex particle methods (Chatelin et al., 2016; Gazzola et al., 2011; Molins et al., 2021), and smoothed particle hydrodynamics (Tartakovsky et al., 2007a; Tartakovsky et al., 2007b; Tartakovsky et al., 2016).

The smoothed particle hydrodynamics (SPH) has been extensively developed by Tartakovsky and co-workers to model reactive transport and mineral precipitation in fractured and porous materials (Tartakovsky et al., 2007a; Tartakovsky et al., 2007b). SPH is a Lagrangian method based on a meshless discretization of partial differential equations. The meshless discretization scheme allows to move the discretization points with fluid velocity, even if the velocity field is highly non-uniform. SPH is Galilean invariant because particle–particle interactions depend on relative particle positions and velocity differences.

The governing equations for the SPH model are as follows: fluid flow and solute diffusion are described by a combination of the continuity equation

$$\frac{\mathrm{d}\rho}{\mathrm{d}t} = -\rho \nabla \cdot \mathbf{u}\,, \tag{52}$$

the linear momentum conservation equation

$$\frac{\mathrm{d}\mathbf{u}}{\mathrm{d}t} = -\frac{1}{\rho}\nabla P + \frac{\mu}{\rho}\nabla^2\mathbf{u} + \frac{1}{\rho}\boldsymbol{F}^{ext}\,, \tag{53}$$

and the diffusion equation

$$\frac{\mathrm{d}C}{\mathrm{d}t} = D\nabla^2 C\,, \tag{54}$$

where $\mathbf{u}$, P, μ, and ρ are the fluid velocity, pressure, viscosity, and density, respectively. The terms, $\boldsymbol{F}^{ext}$ represents the effects of body forces (such as gravity acting on the fluid density), C is the concentration of a solute dissolved in the fluid, and D is the molecular diffusion coefficient of the solute in the solvent. In the SPH approach, both mobile fluids and solid boundaries are represented by particles with intensive properties (e.g., mass m^i) that are tracked in time as they move in the pore space.

In the SPH approach, continuous fields are represented as a superposition of smooth kernel functions centered on point particles. The properties associated with each particle can be expressed as

$$A(\mathbf{r}) = \sum_i \frac{a^i}{n^i} W(\mathbf{r} - \mathbf{r}_i, h) \tag{55}$$

and its corresponding gradient

$$\nabla A(\mathbf{r}) = \sum_i \frac{a^i}{n^i} \nabla_{\mathbf{r}} W(\mathbf{r} - \mathbf{r}_i, h)\,, \tag{56}$$

where a^i is the value of A at particle i. The summation is performed over all the particles.

The mass and momentum conservation equations for each particle in the SPH approximations for continuous fields and their gradients can thus be written in the following form (Tartakovsky et al., 2007a; Tartakovsky et al., 2007b)

$$n^i = \sum_j W(\mathbf{r}_j - \mathbf{r}_i, h) \qquad i, j \in \text{fluid+solid particles} \tag{57}$$

and

$$\frac{\mathrm{d}\mathbf{u}^i}{\mathrm{d}t} = -\frac{1}{m^i}\sum_{j\in \text{fluid+solid}}\left(\frac{P^j}{n^j n^j}+\frac{P^i}{n^i n^i}\right)\nabla_i W(\mathbf{r}_i-\mathbf{r}_j,h) + \frac{1}{m^i}\sum_{j\in \text{fluid+solid}}\frac{(\mu^i+\mu^j)(\mathbf{u}^i-\mathbf{u}^j)}{n^i n^j(\mathbf{r}_i-\mathbf{r}_j)^2}(\mathbf{r}_i-\mathbf{r}_j)\cdot\nabla_i W(\mathbf{r}_i-\mathbf{r}_j,h)+\boldsymbol{F}_i^{ext} \qquad (58)$$

$i \in$ fluid particles

where $\mathbf{r}_i$ is the position of particle i, $n^i = \rho^i/m^i$ is the number density of particle i, ρ^i and m^i are the fluid density and mass of particle i, and h is the range of the SPH smoothing function W. Several forms of weighting function including the Gaussian function (Gingold and Monaghan, 1977) and Schoenberg spline functions of different order (Schoenberg, 1946) can be used in SPH simulations.

Reactive transport is modelled by including the sink/source term in the SPH diffusion equation (Tartakovsky and Meakin, 2005; Zhu and Fox, 2001, 2002) and described by:

$$\frac{\mathrm{d}C^i}{\mathrm{d}t} = \sum_{j\in \text{fluid}}\frac{(D^i n^i + D^j n^j)(C^i-C^j)}{n^i n^j(\mathbf{r}_i-\mathbf{r}_j)^2}(\mathbf{r}_i-\mathbf{r}_j)\cdot\nabla_i W(\mathbf{r}_i-\mathbf{r}_j,h) - R\sum_{k\in \text{solid}}(C^i-C^{eq})\delta_{ik} \qquad (59)$$

The terms, C^i is the solute concentration at fluid particle i, R is the strength of the source or the effective "particle" fluid–solid reaction rate constant. Summation over fluid or solid indicates summation over all the fluid or solid particles. The Kronecker δ_{ik}, which takes the value 1 if $|\mathbf{r}_i-\mathbf{r}_k| \le d$ or 0 otherwise ensures that the precipitation/dissolution occurs only in a thin layer with thickness d near the fluid-solid interface. The last term of this equation is the source term modeling the precipitation or dissolution reaction, and C^{eq} is the solute concentration in equilibrium with the solid.

Precipitation (dissolution) leads to gain (loss) of the solid phase. Consequently, the rate of gain/loss of mass due to precipitation/dissolution of the solid phase must balance the loss/gain of solute in the liquid phase. Thus, the total change of mass of solid particle i, due to interactions with all the fluid particles within distance d, is given by

$$\frac{\mathrm{d}m^i}{\mathrm{d}t} = \frac{R}{n^{eq}}\sum_{j\in \text{fluid}}(C^j-C^{eq})\delta_{ij} \qquad i \in \text{solid} \qquad (60)$$

where n^{eq} is the equilibrium density of the particles. The reactive transport and precipitation model described above conserves the mass of the solute exactly. During precipitation and dissolution, solid particles are added or removed and the change in volume of the fluid phase

should be exactly opposite to that of the solid phase. More details can be found in (Tartakovsky et al., 2007a; Tartakovsky et al., 2007b.

SPH model was used to study the effects of the Damköhler and Peclet numbers on the character of precipitation and changes in the effective transport properties of the porous media (Tartakovsky et al., 2007b). SPH simulations were conducted to help understand the mechanism of precipitation layer formation in a quasi-2D flow cell filled with quartz sand, where two solutions were each injected in different halves of the cell (Tartakovsky et al., 2008).

3.3. COMPUTATIONAL FLUID DYNAMICS METHODS

Many CFD approaches to pore-scale reactive transport modeling have been implemented in the open-source simulation platform OpenFOAM, a C++ library which solves partial differential equations using the finite volume method on an unstructured grid (http://www.openfoam.org). These approaches benefit from all the features offered by the OpenFOAM library, including code parallelization, discretization schemes, and geometric algebraic multigrid solvers. The availability of the open-source software Chombo has also made possible to simulate pore-scale reactive transport processes (Adams et al., 2015; Colella et al., 2000). This section reviews a few of these CFD approaches used for CO_2 applications.

3.3.1. DissolFoam

DissolFoam is a 3D OpenFoam solver for reactive transport with dissolution. It solves for steady flow (Stokes or inertial) and reactant transport.

The reactive transport equations encompass fluid flow, ion advection/diffusion, and chemical reactions at the mineral-fluid interface.

The fluid flow is described by the stationary Navier-Stokes equations:

$$\nabla \cdot (\mathbf{uu}) + \nabla P = \mu \nabla^2 \mathbf{u} \tag{61}$$

Where μ is the viscosity of the fluid and the pressure P is determined by the incompressibility condition,

$$\nabla \cdot \mathbf{u} = 0 \,. \tag{62}$$

Transport of reactants follows a convection-diffusion equation:

$$\frac{\partial C}{\partial t} + \nabla \cdot (\mathbf{u}C) = \nabla \cdot (D \nabla C) \tag{63}$$

Where C is the concentration field and D is the molecular diffusion coefficient.

The steady-state flow and transport are solved by a second-order finite volume discretization of the fields using an unstructured mesh. The governing equations are solved by operator splitting and assume that the velocity of the dissolving mineral surface is much slower than the fluid velocity. Chemical reactions on the mineral surfaces are included by imposing a Robin boundary condition on the surface of the solid. Reaction boundary conditions implemented are linear, non-linear, and danckwerts. The reactive flux only depends on the undersaturation of the aqueous ions. The motion of points on the pore surfaces is controlled by the rate of dissolution. For a detailed description of the method see Starchenko et al. (2016), Starchenko and Ladd (2018), and Dutka et al. (2020). The code is available at https://github.com/vitst/dissolFoam.

3.3.2. GeoChemFoam

GeoChemFoam is an open-source OpenFOAM-based toolbox that includes a range of additional packages that solve various flow processes from multiphase transport with interface transfer, to single-phase flow in multiscale porous media, to reactive transport with mineral dissolution (Maes and Menke, 2021). The multiphase flow is solved using the volume-of-fluid method (VOF), and the transport of species using the continuous species transfer method. The chemical equilibrium is solved with PHREEQC, the U.S. Geological Survey's geochemical software.

The geochemical model is described by the equilibrium chemical reactions between the primary and secondary species, and can be written as

$$A_i \rightleftharpoons \sum_{j=1}^{\bar{N}_c} \nu_{ij} A_j \,, \qquad S_n \rightleftharpoons S_m + \sum_{j=1}^{\bar{N}_c} \nu_{nj} A_j \,, \tag{64}$$

where A_j and A_i are the chemical formulas of the primary and secondary species in the bulk phase, respectively; S_m and S_n are the chemical formulas of the primary and secondary species on the solid surface, respectively; ν_{ij} and ν_{nj} are the stoichiometric coefficients, and $\bar{N}_c$ the number of independent concentrations in the bulk, which also corresponds to the number of chemical elements (e.g., H, O, C).

The total concentration ψ_γ^j for each primary species j in phase γ is conserved during chemical reactions and is given by

$$\psi_\gamma^j = C_\gamma^j + \sum_{i=1}^{N_x} \nu_{ij} C_\gamma^i + \sum_{n=1}^{N_y} \nu_{nj} \omega_n \Gamma A_s \,, \tag{65}$$

where Γ is the site density (kmol/m^2), C_γ^j and C_γ^i are the concentration (kmol/m^3) of primary and secondary species in phase γ, respectively; ω_n is the activity of a surface species n; N_x and N_y are number of secondary bulk and surface species; A_s the specific surface area (m^2/m^3) of the solid which, at the pore-scale, is calculated from the mesh.

The multiphase flow model is described using the VOF method. The single-field momentum equation for a multiphase system can be written as (Maes and Menke, 2021)

$$\frac{\partial \rho \mathbf{u}}{\partial t} + \nabla \cdot (\rho \mathbf{u}\mathbf{u}) = -\nabla P + \nabla \cdot \left(\mu(\nabla \mathbf{u} + \nabla \mathbf{u}^T)\right) + \rho \boldsymbol{g} + \mathbf{f}_{st} \tag{66}$$

where $\boldsymbol{g}$ (m/s^2) is the gravity acceleration and $\mathbf{f}_{st}$ the surface tension force. For a two-phase system, aqueous (phase 1) and non-aqueous (liquid or gas, phase 2) the velocity $\mathbf{u}$ and pressure P in the domain are expressed in terms of the single-field variables as follows

$$\mathbf{u} = \alpha_1 \mathbf{u}_1 + \alpha_2 \mathbf{u}_2 , \quad P = \alpha_1 P_1 + \alpha_2 P_2 \tag{67}$$

where α_1 and $\alpha_2 = 1 - \alpha_1$ are indicator functions used to track the interface between the two fluids, $\mathbf{u}_\gamma$ (m/s) and P_γ (Pa) are the velocity and pressure in phase γ assumed to be Newtonian and incompressible. In the same token, the density and viscosity of the fluid in each cell are expressed as

$$\rho = \alpha_1 \rho_1 + \alpha_2 \rho_2 , \quad \mu = \alpha_1 \mu_1 + \alpha_2 \mu_2 \tag{68}$$

where ρ_γ (kg/m^3) and μ_γ (Pa s) are the density and viscosity of phase γ. The advection of the indicator functions is done by solving the phase transport equation using algebraic VOF methods as described below

$$\frac{\partial \alpha_1}{\partial t} + \nabla \cdot (\alpha_1 \mathbf{u}) + \nabla \cdot (\alpha_1 \alpha_2 \mathbf{u}_r) = -\frac{\dot{m}_{12}}{\rho_1} \tag{69}$$

where $\mathbf{u}_r = \mathbf{u}_1 - \mathbf{u}_2$ is the relative velocity, which is a consequence of mass and momentum transfer between the phases, and $\dot{m}_{12}$ (kg/m^3/s) is the rate of mass transfer from phase 1 to phase 2 by solubility.

For the reactive transport model, the total concentration ψ_γ^j of a primary species j in phase γ must satisfy the conservation equation

$$\frac{\partial \psi_\gamma^j}{\partial t} + \nabla \cdot \left(\psi_\gamma^j \mathbf{u}_\gamma\right) = -\nabla \cdot \mathbf{J}_\gamma^j \tag{70}$$

Where $\mathbf{J}_\gamma^j$ the total diffusive flux of primary species j in phase γ can be modelled using Fick's law

$$\mathbf{J}_\gamma^j = -D_\gamma^j \nabla C_\gamma^j - \sum_{i=1}^{N_x} \nu_{ij} D_\gamma^i \nabla C_\gamma^i \tag{71}$$

The quantities D_γ^j and D_γ^i are the molecular diffusion coefficients (m^2/s) of the primary and secondary species in phase γ.

Within the VOF method, the reactive transport equations are integrated over a control volume using volume averaging (Maes and Soulaine, 2020) and boundary conditions. Due to the difficulty of developing an accurate and stable transport solver for the total concentrations $\left(\psi^j\right)_{1\le j\le \bar{N}_c}$, the numerical model solves directly for the concentration of the primary and secondary species using a sequential non-iterative operator splitting approach (Carrayrou et al., 2004). The transport step solves the single-field transport equation using the continuous species transfer (CST) method (Maes and Soulaine, 2020).

$$\frac{\partial C^k}{\partial t} + \nabla \cdot (C^k \mathbf{u}) + \nabla \cdot \left(\alpha_1 \alpha_2 \left(C_1^k - C_2^k\right)\mathbf{u}_r\right) - \nabla \cdot (D^k \nabla C^k - \mathbf{\Phi}_k) = 0 \tag{72}$$

where $\mathbf{\Phi}_k$ is the CST flux of species k, D^k the single-field diffusion coefficient of species k, and C^k the single-field concentration of species k (primary or secondary) with $C^k = \alpha_1 C_1^k + \alpha_2 C_2^k$. The boundary condition at the surface of the solid for the single-field concentration of species k is defined by Graveleau et al. (2017)

$$D^k \nabla C^k - \mathbf{\Phi}_k = 0 \tag{73}$$

For more details of the model derivation and implementation see Maes and Menke (2021). For the code availability go to https://www.julienmaes.com/geochemfoam.

The code was applied to simulate multiphase reactive transport in a micro-CT image of Bentheimer sandstone where a solution of $CaCl_2$ was injected into an oil saturated domain with surface complexation at the solid surface. Other fields of applications are in the oil and gas, carbon capture and storage, contaminant transport, battery, and fuel cell industries (Maes and Menke (2021).

3.3.3. CrunchFoam

CrunchFoam is a pore-scale multiphase reactive transport modeling framework developed by coupling the open source software package OpenFOAM and the geochemical reaction solver CrunchTope (Li et al., 2022). The coupling is done through a generic interface, Alquimia, that exposes the capabilities of existing and thoroughly validated geochemistry codes (Andre et al.,

2013). CrunchFoam solves two-phase flow, transport, and geochemical reactions sequentially using the operator splitting approach. The time stepping is controlled by the flow solver in OpenFOAM.

The two-phase flow is solved using the standard OpenFOAM solver for transient incompressible isothermal flow of two immiscible fluids, interFoam, which implements a modified version of the VOF method by treating the two fluid phases as an effective single phase. In this approach, the velocity and pressure fields are solved by the single-field incompressible Navier-Stokes equation and continuity equation (Hirt and Nichols, 1981). The transport is solved using the compressive-continuous species transfer method, where the transport of a species j dissolved in both phases is described as follows (Maes and Soulaine, 2018)

$$\frac{\partial C^j}{\partial t} + \nabla \cdot \left(\mathbf{u} C^j\right) = -\nabla \cdot \left(\frac{\left(1 - H^j\right) C^j}{\alpha + (1-\alpha) H^j} \alpha (1-\alpha) \mathbf{u}_r \right) + \nabla \cdot \left(\widehat{D}^j \nabla C^j + \Psi^j \right) + R^j \qquad (74)$$

where $\widehat{D}^j$ is the interpolation of the diffusion coefficient of the chemical species in the two phases, Ψ^j is the concentration jump at the interface, H^j is the Henry's law constant, C^j is the concentration of species j, $\mathbf{u}$ is the velocity, $\mathbf{u}_r$ the relative velocity between the two fluids/phases, and α the volume fraction of a designated fluid. The reaction rate R^j is described by the transition state theory rate law.

CrunchFOAM was applied to investigate pore-scale dynamics of two-phase flow and their impacts on mineral reaction rates (Li et al., 2022).

3.3.4. Chombo-Crunch

Chombo-Crunch is a code suite developed since 2010 by Trebotich and co-workers to simulate subsurface flow and reactive transport at the pore-scale by direct numerical simulation techniques (Molins et al. 2017; Molins et al., 2012; Molins et al. 2014). It is a combination of the high-performance Chombo software package (Trebotich et al., 2008) for flow, transport, and geometry evolution processes with the geochemical reactions code CrunchFlow (Steefel et al., 2015; Steefel and Molins, 2009).

The governing equations are the Navier-Stokes equations for incompressible flow and the advection-diffusion reaction equations for the transport of aqueous species:

$$\frac{\partial \mathbf{u}}{\partial t} + (\mathbf{u} \cdot \nabla)\mathbf{u} + \frac{1}{\rho}\nabla P = \nu \nabla^2 \mathbf{u} \qquad (75)$$

$$\nabla \cdot \mathbf{u} = 0 \qquad (76)$$

$$\frac{\partial C}{\partial t} + \nabla \cdot (\mathbf{u} C) = \nabla \cdot (D \nabla C) \qquad (77)$$

Where ρ, ν, P, and $\mathbf{u}$ are the fluid density, the kinematic viscosity, the fluid pressure, and the fluid velocity, respectively; C is the concentration of the dissolved component and D is the molecular diffusion coefficient. Mineral dissolution, described as a kinetic process, takes place at the fluid-solid interface, and can be expressed as a Robin boundary condition on the transport equation

$$-D\mathbf{n} \cdot \nabla C = \xi r \tag{78}$$

With $\mathbf{n}$ the outward surface normal to the fluid region, r the mineral dissolution rate which is described explicitly as a function of the species concentrations, and ξ the stoichiometric coefficient of species in the dissolution reaction.

Geochemical reactions are coupled to transport using an operator splitting approach. The code uses an embedded boundary-algebraic multigrid formulation based on a finite volume discretization where the solid−fluid interfaces are represented with embedded boundaries within each of the Cartesian grid cells. Conservation equations are solved using a predictor-corrector projection method. To minimize numerical dispersion, a higher order upwind method with a van Leer flux limiter is applied to advection terms in a semi-implicit Crank-Nicolson approach. More details can be found at Molins et al. (2017, 2012, 2014).

Chombo-Crunch was applied to investigate the pore-scale transport and surface reaction controls on calcite dissolution under elevated pCO_2 conditions (Molins et al. (2014).

4. HYBRID-SCALE MODELS

Hybrid-scale models describe systems that include multiple characteristic length-scales, where some regions are described using pore-scale modelling and others are modelled with continuum approaches. Two different approaches have been developed to solve hybrid-scale problems: the domain decomposition technique and the micro-continuum models.

The domain decomposition technique solves different physics on separate domains, one for Darcy flow and the other for Stokes flow. The domains are linked together through appropriate boundary conditions (Molins et al., 2019).

The micro-continuum models use a single set of partial differential equations (e.g., Darcy-Brinkman-Stokes equation) throughout the computational domain (Soulaine and Tchelepi, 2016; Steefel et al., 2015).

An example of a hybrid-scale model reactive transport code is *porousMedia4Foam* (Soulaine et al., 2021).

4.1. POROUSMEDIA4FOAM

porousMedia4Foam is a multi-scale open-source package to solve flow and transport in porous media within the simulation platform OpenFOAM (Soulaine et al., 2021). It is built using PHREEQC, an open-source and popular geochemistry package used in many continuum-scale reactive transport modeling. It relies on micro-continuum concept and makes it possible to investigate hydro-geochemical processes occurring at multiple scales, i.e., at the pore-scale, reservoir (or continuum)-scale, and at the hybrid-scale. The source code is available on GitHub (https://github.com/csoulain/porousMedia4Foam). Although the package has capabilities for solving two-phase flow (liquid-liquid and liquid-gas) in porous systems, the geochemistry coupling introduced in their paper only considers single-phase flow.

porousMedia4Foam includes three flow models: a multi-scale flow solver (that includes pore-scale, hybrid-scale, continuum-scale) based on the micro-continuum approach, and a continuum-scale Darcy solver and a constant velocity solver.

Micro-continuum approaches are intermediate between a pure Navier-Stokes description of the transport for which all the porosity is fully resolved, and a pure continuum-scale modelling for which the flow is governed by Darcy's law. The momentum equation which arises from the integration of the Navier-Stokes equation over a control volume (Bennon and Incropera, 1987; Bousquet-Melou et al., 2002; Goyeau et al., 2003; Quintard and Whitaker, 1999; Vafai and Tien, 1981) is given by:

$$\frac{1}{\phi}\left(\frac{\partial \rho_f \mathbf{u}}{\partial t} + \nabla \cdot \left(\frac{\rho_f}{\phi}\mathbf{u}\mathbf{u}\right)\right) = -\nabla P_f + \rho_f \boldsymbol{g} + \nabla \cdot \left(\frac{\mu_f}{\phi}\left(\nabla \mathbf{u} + {}^{t}\nabla \mathbf{u}\right)\right) - \mu_f k^{-1}\mathbf{u} \tag{79}$$

Where ϕ, $\mathbf{u}$, P_f, $\boldsymbol{g}$, ρ_f, μ_f, and k are the porosity, the seepage velocity (m/s), the fluid pressure (Pa), the gravity (m/s^2), the fluid density (kg/m^3), the fluid viscosity (Pa s), and the cell permeability (m^2), respectively. The porous media properties, including porosity and

permeability, change dynamically with geochemical processes and are updated at every time step. The porosity field is computed by

$$\phi = 1 - \sum_{i}^{N_S - 1} Y_S^i - Y_S^{inert} , \tag{80}$$

Y_S^i is the volume fraction of mineral *i* on the computational grid, Y_S^{inert} defines an inert mineral and N_s the number of minerals.

In *porousMedia4Foam*, complex reaction networks are handled by geochemical packages. Four models are currently implemented to account for the geochemistry (Table 2). The geochemical packages update the water composition C^j, and the distribution of the solid minerals Y_S^i , and return the rate of solid changes,

$$\dot{m}_S^i = \frac{\partial \rho_S^i Y_S^i}{\partial t} \tag{81}$$

where ρ_S^i is the density of solid mineral *i*.

In the PHREEQC model, the coupling between transport and reactions relies on an operator-splitting approach based on the Strang's algorithm (Strang, 1968). All species concentration fields, C^j, are transported sequentially using the advection-dispersion equations,

$$\frac{\partial \phi C^j}{\partial t} + \nabla \cdot \left(\mathbf{u} C^j\right) - \nabla \cdot \left(\phi D^{*j} \cdot \nabla C^j\right) = 0 , \tag{82}$$

D^{*j} is an effective diffusion tensor that accounts for tortuosity and hydrodynamic dispersion effects. The fluid velocity **u** is computed with the flow solver.

The first order kinetic model solves the transport of single species that reacts with solid minerals using first order kinetic reactions. Considering a chemical reaction where species A reacts with a mineral to produce species B, the mass balance equation for species A can be written as:

$$\frac{\partial \phi C^A}{\partial t} + \nabla \cdot (\mathbf{u} C^A) - \nabla \cdot \left(\phi D^{*j} \cdot \nabla C^A\right) = -\left(\sum_{j=1}^{N_S} A_S^j \left(k_{j,A} \gamma_A\right)\right) C^A , \tag{83}$$

where A_S^j (m^{-1}) is the reactive surface area of mineral j, and $\left(k_{j,A}\gamma_A\right)$ in m/s is the constant of reaction of the species A with the mineral j. The concentration field C^j is in mol/m^3. The distribution of solid minerals evolves according to

$$\frac{\partial Y_s^i}{\partial t} = -A_s^A\left(k_{i,A}\gamma_A\right)V_{m_{s,i}}C^A\,, \tag{84}$$

$V_{m_{s,i}}$ (m^3/mol) is the molar volume of the reacting mineral.

The other two models of the geochemical packages are transport only (no geochemistry, advection-dispersion equation is solved) and flow only (no transport and no geochemistry).

Porous media models are generally described by their properties including absolute permeability, specific surface area, and dispersion tensor. Several models have been implemented in the code (Table 2).

Table 2: Summary of the Geochemical Packages for Hydro-Geochemical Processes, Permeability-Porosity Models, Specific Surface Area Models, and Dispersion Models Implemented in porousMedia4Foam. See Appendix for their expressions.

	Geochemical Packages	Permeability-Porosity	Surface Area	Dispersion
Model	PHREEQC First order kinetic Transport only Flow only	None Constant Power-law Kozeny-Carman Verma-Singh Hele-Shaw	None Constant Volume of solid Power-law Sugar lump Hydro-geochemical coupling	None Diffusion only Archie's Law Linear dispersion

The permeability-porosity models implemented include None, Constant (uniform or non-uniform), Power-law (permeability power law of porosity), Kozeny-Carman, Verma-Pruess, and Hele-Shaw.

The specific surface area models implemented in porousMedia4Foam are the following: None (e.g., for phase equilibrium calculation), Constant surface area, Volume of solid (for pore-scale simulations only, local surface area computed based on the mineral mapping), Power-law (power of the distribution of the solid minerals), Sugar lump (evolution of the surface area of an aggregate during dissolution), and Hydro-geochemical coupling.

For the dispersion, four models are implemented including: None (model transport by advection only), Diffusion only (no tortuosity effects, no hydrodynamic dispersion), Archie's Law (tortuosity represented by a power law of porosity), and Linear dispersion.

The application fields of this package include the investigation of hydro-bio-geochemical processes in the critical zone, the modelling of contaminant transport in aquifers, and the assessment of confinement performance for geological barriers (Soulaine et al., 2021).

5. CONCLUSIONS

Accurate modelling and prediction of subsurface processes involving flow, transport, and geochemical reactions requires advanced tools and approaches. Reactive transport modelling consists of computational approaches and numerical models that describe the coupled physical, chemical, mechanical, and biological processes interacting with each other over a broad range of spatial and temporal scales. Three different kinds of approaches for CO_2 applications have been defined: continuum-scale approach based on Darcy equation, pore-scale approach, and hybrid-scale approach. All three approaches have been presented in this work and a few examples of reactive transport codes have been described.

The continuum-scale approach deals with problems at the macroscale and relies on average quantities over a REV and constitutive relationships, but fails to describe the microscopic insights of the porous media. The pore-scale approach requires an exact knowledge of the phase distribution and computes properties of the system at the microscopic level that can be used to determine properties at the continuum-scale. The hybrid-scale approach bridges the gap between the continuum- and pore-scale approach, where some regions of the porous media are treated at the Darcy-scale while others at the pore-scale. However, the last two approaches are still emerging.

Reactive transport codes differ not only by their approaches, but also by their features, capabilities, and license requirements. A few of these codes have the design capability to simulate multiphase flow, multiphase reactive transport, or geo-mechanics. While many of them are open-source codes (or free for DOE laboratories), others require the purchase of a license.

It is important to determine the best approach and model to solve a particular/specific problem and the influence of the model on the results. This work will provide guidance on choosing appropriate approaches, and therefore, reactive transport codes to solve a particular problem.

6. REFERENCES

Adams, M.; Colella, P.; Graves, D. T.; Johnson, J.; Keen, N.; Ligocki, T. J.; . . . Straalen, B. *Chombo software package for AMR applications-design document*; Technical Report LBNL-6616E; Lawrence Berkeley National Laboratory; 2015.

Amos, R. T.; Mayer, K. U. Investigating Ebullition in a Sand Column Using Dissolved Gas Analysis and Reactive Transport Modeling. *Environmental Science & Technology* **2006a,** *40*, 5361–5367. doi:10.1021/es0602501

Amos, R. T.; Mayer, K. U. Investigating the role of gas bubble formation and entrapment in contaminated aquifers: Reactive transport modelling. *Journal of Contaminant Hydrology* **2006b,** *87*, 123–154. doi:https://doi.org/10.1016/j.jconhyd.2006.04.008

Andre, B.; Molins, S.; Johnson, J.; Steefel, C.; USDOE. Alquimia. United States, 2013. https://www.osti.gov/biblio/1231758

Arora, B.; Şengör, S. S.; Spycher, N. F.; Steefel, C. I. A reactive transport benchmark on heavy metal cycling in lake sediments. *Computational Geosciences* **2015,** *19*, 613–633. doi:10.1007/s10596-014-9445-8

Bacon, D. H.; Qafoku, N. P.; Dai, Z.; Keating, E. H.; Brown, C. F. Modeling the impact of carbon dioxide leakage into an unconfined, oxidizing carbonate aquifer. *International Journal of Greenhouse Gas Control* ***2016,*** *44*, 290–299. doi:https://doi.org/10.1016/j.ijggc.2015.04.008

Bacon, D. H.; Yonkofski, C. M. R.; Schaef, H. T.; White, M. D.; McGrail, B. P. CO_2 storage by sorption on organic matter and clay in gas shale. *Journal of Unconventional Oil and Gas Resources* **2015,** *12*, 123–133. doi:https://doi.org/10.1016/j.juogr.2015.09.004

Bagheri, M.; Shariatipour, S. M.; Ganjian, E. Prediction of the lifespan of cement at a specific depth based on the coupling of geomechanical and geochemical processes for CO_2 storage. *International Journal of Greenhouse Gas Control* **2019,** *86*, 43–65. doi:https://doi.org/10.1016/j.ijggc.2019.04.016

Bea, S.; Mayer, K.; MacQuarrie, K. *Modelling reactive transport in sedimentary rock environments-Phase II MIN3P-THCm code enhancements and illustrative simulations for a glaciation scenario*; Technical Report NWMO TR-2011-13; 2011.

Bea, S. A.; Mayer, U.; MacQuarrie, K. Reactive transport and thermo-hydro-mechanical coupling in deep sedimentary basins affected by glaciation cycles: model development, verification, and illustrative example. *Geofluids* **2016,** *16*, 279–300.

Bea, S. A.; Wilson, S. A.; Mayer, K. U.; Dipple, G. M.; Power, I. M.; Gamazo, P. Reactive Transport Modeling of Natural Carbon Sequestration in Ultramafic Mine Tailings. *Vadose Zone Journal* **2012,** *11*. doi:10.2136/vzj2011.0053

Bear, J.; Bachmat, Y. *Introduction to modeling of transport phenomena in porous media*; Springer Science & Business Media; 2012; Vol 4.

Benisch, K.; Graupner, B.; Bauer, S. The coupled OpenGeoSys-eclipse simulator for simulation of CO_2 storage–code comparison for fluid flow and geomechanical processes. *Energy Procedia* **2013,** *37*, 3663–3671.

Benisch, K.; Wang, W.; Delfs, J.-O.; Bauer, S. The OGS-Eclipse code for simulation of coupled multiphase flow and geomechanical processes in the subsurface. *Computational Geosciences* **2020,** *24*, 1315–1331.

Bennon, W.; Incropera, F. A continuum model for momentum, heat and species transport in binary solid-liquid phase change systems—I. Model formulation. *International Journal of Heat and Mass Transfer* **1987,** *30*, 2161–2170.

Berner, U.; Kulik, D. A.; Kosakowski, G. Geochemical impact of a low-pH cement liner on the near field of a repository for spent fuel and high-level radioactive waste. *Physics and Chemistry of the Earth, Parts A/B/C* **2013,** *64*, 46–56. doi:https://doi.org/10.1016/j.pce.2013.03.007

Beyer, C.; Li, D.; De Lucia, M.; Kühn, M.; Bauer, S. Modelling CO_2-induced fluid–rock interactions in the Altensalzwedel gas reservoir. Part II: coupled reactive transport simulation. *Environmental Earth Sciences* **2012,** *67*, 573–588.

Beyer, C.; Popp, S.; Bauer, S. Simulation of temperature effects on groundwater flow, contaminant dissolution, transport and biodegradation due to shallow geothermal use. *Environmental Earth Sciences* **2016,** *75*, 1–20.

Bhatnagar, P. L.; Gross, E. P.; Krook, M. A Model for Collision Processes in Gases. I. Small Amplitude Processes in Charged and Neutral One-Component Systems. *Physical Review* **1954,** *94*, 511–525. doi:10.1103/PhysRev.94.511

Bilardi, S.; Amos, R. T.; Blowes, D. W.; Calabrò, P. S.; Moraci, N. Reactive Transport Modeling of ZVI Column Experiments for Nickel Remediation. *Groundwater Monitoring & Remediation* **2013,** *33*, 97–104. doi:https://doi.org/10.1111/j.1745-6592.2012.01417.x

Bildstein, O.; Kervévan, C.; Lagneau, V.; Delaplace, P.; Crédoz, A.; Audigane, P.; . . . Jullien, M. Integrative modeling of caprock integrity in the context of CO_2 storage: evolution of transport and geochemical properties and impact on performance and safety assessment. *Oil & Gas Science and Technology–Revue de l'Institut Français du Pétrole* **2010,** *65*, 485–502.

Böttcher, N.; Singh, A.-K.; Kolditz, O.; Liedl, R. Non-isothermal, compressible gas flow for the simulation of an enhanced gas recovery application. *Journal of Computational and Applied Mathematics* **2012,** *236*, 4933–4943.

Bousquet-Melou, P.; Goyeau, B.; Quintard, M.; Fichot, F.; Gobin, D. Average momentum equation for interdendritic flow in a solidifying columnar mushy zone. *International Journal of Heat and Mass Transfer* **2002,** *45*, 3651–3665.

Carman, P. C. Fluid flow through granular beds. *Transactions of the Institution of Chemical Engineers* **1937,** *15*, 150–166.

Carrayrou, J.; Mosé, R.; Behra, P. Operator-splitting procedures for reactive transport and comparison of mass balance errors. *Journal of Contaminant Hydrology* **2004,** *68*, 239–268. doi:https://doi.org/10.1016/S0169-7722(03)00141-4

Centler, F.; Shao, H.; De Biase, C.; Park, C.-H.; Regnier, P.; Kolditz, O.; Thullner, M. GeoSysBRNS—A flexible multidimensional reactive transport model for simulating biogeochemical subsurface processes. *Computers & Geosciences* **2010,** *36*, 397–405.

Chatelin, R.; Sanchez, D.; Poncet, P. Analysis of the penalized 3D variable viscosity stokes equations coupled to diffusion and transport. *ESAIM: M2AN* **2016,** *50*, 565–591. https://doi.org/10.1051/m2an/2015056

Chen, L.; Kang, Q.; Tang, Q.; Robinson, B. A.; He, Y.-L.; Tao, W.-Q. Pore-scale simulation of multicomponent multiphase reactive transport with dissolution and precipitation. *International Journal of Heat and Mass Transfer* **2015,** *85*, 935–949. doi:https://doi.org/10.1016/j.ijheatmasstransfer.2015.02.035

Cheng, L. Dual porosity reactive transport modeling. PhD Thesis, University of Sheffield, 2005.

Cheng, L.; Lerner, D.; Thornton, S.; Ulrich Mayer, K. MTBE attenuation in a dual porosity chalk aquifer-field observations and modelling results. *IAHS-AISH Publication* **2011,** *341*, 159–165.

Claret, F.; Marty, N.; Tournassat, C. Modeling the long-term stability of multi-barrier systems for nuclear waste disposal in geological clay formations. Reactive Transport Modeling: Applications in Subsurface Energy, and Environmental Problems; John Wiley & Sons, Ltd: Chichester, UK, 2018; p. 395–451.

Colella, P.; Graves, D. T.; Ligocki, T. J.; Miller, G. H.; Modiano, D.; Schwartz, P.; . . . Barad, M. EBChombo Software Package for Cartesian Grid, Embedded Boundary Applications: Technical Report LBNL-6615E; Lawrence Berkeley National Laboratory; 2000.

Curti, E.; Xto, J.; Borca, C. N.; Henzler, K.; Huthwelker, T.; Prasianakis, N. I. Modelling Ra-bearing baryte nucleation/precipitation kinetics at the pore scale: application to radioactive waste disposal. *European Journal of Mineralogy* **2019,** *31*, 247–262. doi:10.1127/ejm/2019/0031-2818

d'Humières, D.; Lallemand, P.; Frisch, U. Lattice Gas Models for 3D Hydrodynamics. *Europhysics Letters (EPL)* **1986,** *2*, 291–297. doi:10.1209/0295-5075/2/4/006

De Biase, C.; Maier, U.; Oswald, S.; Thullner, M. Reactive transport simulation of volatile organic compound removal in vertical flow soil filters. *IAHS-AISH Publication* **2012,** *355*, 169–174.

De Windt, L.; Badreddine, R.; Lagneau, V. Long-term reactive transport modelling of stabilized/solidified waste: from dynamic leaching tests to disposal scenarios. *Journal of Hazardous Materials* **2007,** *139*, 529–536. doi:https://doi.org/10.1016/j.jhazmat.2006.03.045

DePaolo, D. J.; Cole, D. R. Geochemistry of geologic carbon sequestration: an overview. *Reviews in Mineralogy and Geochemistry* **2013,** *77*, 1–14.

Dobson, P. F.; Kneafsey, T. J.; Sonnenthal, E. L.; Spycher, N.; Apps, J. A. Experimental and numerical simulation of dissolution and precipitation: implications for fracture sealing at Yucca Mountain, Nevada. *Journal of Contaminant Hydrology* **2003,** *62*, 459–476.

Drawert, B.; Jacob, B.; Li, Z.; Yi, T.-M.; Petzold, L. A hybrid smoothed dissipative particle dynamics (SDPD) spatial stochastic simulation algorithm (sSSA) for advection–diffusion–reaction problems. *Journal of Computational Physics* **2019,** *378*, 1–17. doi:https://doi.org/10.1016/j.jcp.2018.10.043

Dutka, F.; Starchenko, V.; Osselin, F.; Magni, S.; Szymczak, P.; Ladd, A. J. C. Time-dependent shapes of a dissolving mineral grain: Comparisons of simulations with microfluidic experiments. *Chemical Geology* **2020,** *540*, 119459. doi:https://doi.org/10.1016/j.chemgeo.2019.119459

Forde, O. N.; Mayer, K. U.; Cahill, A. G.; Mayer, B.; Cherry, J. A.; Parker, B. L. Vadose Zone Gas Migration and Surface Effluxes after a Controlled Natural Gas Release into an Unconfined Shallow Aquifer. *Vadose Zone Journal* **2018,** *17*, 180033. doi:https://doi.org/10.2136/vzj2018.02.0033

Frisch, U.; Hasslacher, B.; Pomeau, Y. Lattice-Gas Automata for the Navier-Stokes Equation. *Physical Review Letters* **1986,** *56*, 1505–1508. doi:10.1103/PhysRevLett.56.1505

Gaus, I.; Azaroual, M.; Czernichowski-Lauriol, I. Reactive transport modelling of the impact of CO_2 injection on the clayey cap rock at Sleipner (North Sea). *Chemical Geology* **2005,** *217*, 319–337.

Gazzola, M.; Chatelain, P.; Van Rees, W. M.; Koumoutsakos, P. Simulations of single and multiple swimmers with non-divergence free deforming geometries. *Journal of Computational Physics* **2011,** *230*, 7093–7114.

Gingold, R. A.; Monaghan, J. J. Smoothed particle hydrodynamics: theory and application to non-spherical stars. *Monthly Notices of the Royal Astronomical Society* **1977,** *181*, 375–389. doi:10.1093/mnras/181.3.375

Goerke, U.-J.; Park, C.-H.; Wang, W.; Singh, A.; Kolditz, O. Numerical simulation of multiphase hydromechanical processes induced by CO_2 injection into deep saline aquifers. *Oil & Gas Science and Technology–Revue d'IFP Energies Nouvelles* **2011,** *66*, 105–118.

Goyeau, B.; Lhuillier, D.; Gobin, D.; Velarde, M. Momentum transport at a fluid–porous interface. *International Journal of Heat and Mass Transfer* **2003,** *46*, 4071–4081.

Graupner, B. J.; Li, D.; Bauer, S. The coupled simulator ECLIPSE–OpenGeoSys for the simulation of CO_2 storage in saline formations. *Energy Procedia* **2011,** *4*, 3794–3800.

Graveleau, M.; Soulaine, C.; Tchelepi, H. A. Pore-scale simulation of interphase multicomponent mass transfer for subsurface flow. *Transport in Porous Media* **2017,** *120*, 287–308.

Hammond, G. E.; Lichtner, P. C.; Mills, R. Evaluating the performance of parallel subsurface simulators: An illustrative example with PFLOTRAN. *Water Resources Research* **2014,** *50*, 208–228.

Harrison, A. L.; Dipple, G. M.; Power, I. M.; Mayer, K. U. Influence of surface passivation and water content on mineral reactions in unsaturated porous media: Implications for brucite carbonation and CO2 sequestration. *Geochimica et Cosmochimica Acta* **2015,** *148*, 477–495. doi:https://doi.org/10.1016/j.gca.2014.10.020

He, X.; Luo, L.-S. A priori derivation of the lattice Boltzmann equation. *Physical Review E* **1997,** *55*, R6333–R6336. doi:10.1103/PhysRevE.55.R6333

Heldt, S.; Wang, B.; Hu, L.; Hornbruch, G.; Lueders, K.; Werban, U.; Bauer, S. Numerical investigation of a high temperature heat injection test. *Journal of Hydrology* **2021,** *597*, 126229.

Henderson, T. H.; Mayer, K. U.; Parker, B. L.; Al, T. A. Three-dimensional density-dependent flow and multicomponent reactive transport modeling of chlorinated solvent oxidation by potassium permanganate. *Journal of Contaminant Hydrology* **2009,** *106*, 195–211. doi:https://doi.org/10.1016/j.jconhyd.2009.02.009

Hers, I.; Jourabchi, P.; Lahvis, M. A.; Dahlen, P.; Luo, E. H.; Johnson, P.; . . . Mayer, K. U. Evaluation of Seasonal Factors on Petroleum Hydrocarbon Vapor Biodegradation and Intrusion Potential in a Cold Climate. *Groundwater Monitoring & Remediation* **2014,** *34*, 60–78. doi:https://doi.org/10.1111/gwmr.12085

Higuera, F. J.; Jiménez, J. Boltzmann Approach to Lattice Gas Simulations. *Europhysics Letters (EPL)* **1989,** *9*, 663–668. doi:10.1209/0295-5075/9/7/009

Hirt, C. W.; Nichols, B. D. Volume of fluid (VOF) method for the dynamics of free boundaries. *Journal of Computational Physics* **1981,** *39*, 201–225. doi:https://doi.org/10.1016/0021-9991(81)90145-5

Huber, C., Shafei, B., & Parmigiani, A. A new pore-scale model for linear and non-linear heterogeneous dissolution and precipitation. *Geochimica et Cosmochimica Acta* **2014,** *124*, 109–130. doi:https://doi.org/10.1016/j.gca.2013.09.003

INAP. The global acid rock drainage guide. The International Network for Acid Prevention; 2009. http://www.gardguide.com/index.php/Chapter_1

Jamieson-Hanes, J. H.; Amos, R. T.; Blowes, D. W. Reactive transport modeling of chromium isotope fractionation during Cr (VI) reduction. *Environmental Science & Technology* **2012,** *46*, 13311–13316.

Jia, M.; Jacques, D.; Gérard, F.; Su, D.; Mayer, K. U.; Šimůnek, J. A benchmark for soil organic matter degradation under variably saturated flow conditions. *Computational Geosciences* **2021,** *25*, 1359–1377. doi:10.1007/s10596-019-09862-3

Ju, X.; Liu, F.; Fu, P.; White, M. D.; Settgast, R. R.; Morris, J. P. Gas Production from Hot Water Circulation through Hydraulic Fractures in Methane Hydrate-Bearing Sediments: THC-Coupled Simulation of Production Mechanisms. *Energy & Fuels* **2020,** *34*, 4448–4465. doi:10.1021/acs.energyfuels.0c00241

Kang, Q.; Lichtner, P. C.; Viswanathan, H. S.; Abdel-Fattah, A. I. Pore Scale Modeling of Reactive Transport Involved in Geologic CO_2 Sequestration. *Transport in Porous Media* **2010,** *82*, 197–213. doi:10.1007/s11242-009-9443-9

Kang, Q.; Lichtner, P. C.; Zhang, D. Lattice Boltzmann pore-scale model for multicomponent reactive transport in porous media. *Journal of Geophysical Research: Solid Earth* **2006,** *111*. doi:https://doi.org/10.1029/2005JB003951

Kang, Q.; Lichtner, P. C.; Zhang, D. An improved lattice Boltzmann model for multicomponent reactive transport in porous media at the pore scale. *Water Resources Research* **2007,** *43*. doi:https://doi.org/10.1029/2006WR005551

Kim, J.; Sonnenthal, E.; Rutqvist, J. A sequential implicit algorithm of chemo-thermo-poro-mechanics for fractured geothermal reservoirs. *Computers & Geosciences* **2015,** *76*, 59–71. doi:https://doi.org/10.1016/j.cageo.2014.11.009

Kolditz, O.; Bauer, S. A process-oriented approach to computing multi-field problems in porous media. *Journal of Hydroinformatics* **2004,** *6*, 225–244.

Kolditz, O.; Bauer, S.; Bilke, L.; Böttcher, N.; Delfs, J.-O.; Fischer, T.; . . . McDermott, C. OpenGeoSys: an open-source initiative for numerical simulation of thermo-hydro-mechanical/chemical (THM/C) processes in porous media. *Environmental Earth Sciences* **2012a,** *67*, 589–599.

Kolditz, O.; Görke, U.-J.; Shao, H.; Wang, W. *Thermo-Hydro-Mechanical-Chemical Processes in Porous Media - Benchmarks and Examples*, 1 ed.; Springer Berlin: Heidelberg; 2012b.

Kolditz, O.; Görke, U.-J.; Shao, H.; Wang, W.; Bauer, S. *Thermo-Hydro-Mechanical-Chemical Processes in Fractured Porous Media: Modelling and Benchmarking - Benchmarking Initiatives*, 1 ed.; Springer International Publishing Switzerland: Springer Cham., 2016.

Kolditz, O.; Nagel, T.; Shao, H.; Wang, W.; Bauer, S. *Thermo-Hydro-Mechanical-Chemical Processes in Fractured Porous Media: Modelling and Benchmarking - From Benchmarking to Tutoring*, 1 ed.; Springer International Publishing AG: Springer Cham., 2018.

Kolditz, O.; Shao, H.; Wang, W.; Bauer, S. *Thermo-Hydro-Mechanical-Chemical Processes in Fractured Porous Media: Modelling and Benchmarking - Closed-Form Solutions*, 1 ed.; Springer International Publishing Switzerland: Springer Cham., 2015.

Kozeny, J. Uber kapillare leitung der wasser in boden. *Royal Academy of Science, Vienna, Proc. Class I* **1927,** *136*, 271-306.

Li, L.; Salehikhoo, F.; Brantley, S. L.; Heidari, P. Spatial zonation limits magnesite dissolution in porous media. *Geochimica et Cosmochimica Acta* **2014,** *126*, 555–573. doi:https://doi.org/10.1016/j.gca.2013.10.051

Li, P.; Deng, H.; Molins, S. The Effect of Pore-Scale Two-Phase Flow on Mineral Reaction Rates. *Frontiers in Water* **2022,** *188*.

Lichtner, P.; Hammond, G.; Lu, C.; Karra, S.; Bisht, G.; Andre, B.; . . . Frederick, J. PFLOTRAN User Manual; 2020a. http://documentation.pflotran.org

Lichtner, P.; Hammond, G.; Lu, C.; Karra, S.; Bisht, G.; Andre, B.; . . . Frederick, J. PFLOTRAN Webpage, 2020b. http://www.pflotran.org

Liu, I.-S. *Continuum Mechanics*; Springer-Verlag.: Berlin, 2002.

Maes, J.; Menke, H. P. GeoChemFoam: Direct Modelling of Multiphase Reactive Transport in Real Pore Geometries with Equilibrium Reactions. *Transport in Porous Media* **2021,** *139*, 271–299. doi:10.1007/s11242-021-01661-8

Maes, J.; Soulaine, C. A new compressive scheme to simulate species transfer across fluid interfaces using the Volume-Of-Fluid method. *Chemical Engineering Science* **2018,** *190*, 405–418. doi:https://doi.org/10.1016/j.ces.2018.06.026

Maes, J.; Soulaine, C. A unified single-field Volume-of-Fluid-based formulation for multi-component interfacial transfer with local volume changes. *Journal of Computational Physics* **2020,** *402*, 109024. doi:https://doi.org/10.1016/j.jcp.2019.109024

Massoudi, M. *Heat transfer in complex fluids*; INTECH Open Access Publisher; 2011.

Matos de Souza, M.; Oostrom, M.; White, M. D.; Cardoso da Silva, G.; Barbosa, M. C. Simulation of Subsurface Multiphase Contaminant Extraction Using a Bioslurping Well Model. *Transport in Porous Media* **2016,** *114*, 649-673. doi:10.1007/s11242-016-0738-3

Mayer, K. U.; Alt-Epping, P.; Jacques, D.; Arora, B.; Steefel, C. I. Benchmark problems for reactive transport modeling of the generation and attenuation of acid rock drainage. *Computational Geosciences* **2015,** *19*, 599–611. doi:10.1007/s10596-015-9476-9

Mayer, K. U.; Benner, S. G.; Blowes, D. W. Process-based reactive transport modeling of a permeable reactive barrier for the treatment of mine drainage. *Journal of Contaminant Hydrology* **2006,** *85*, 195–211. doi:https://doi.org/10.1016/j.jconhyd.2006.02.006

Mayer, K. U.; Frind, E. O.; Blowes, D. W. Multicomponent reactive transport modeling in variably saturated porous media using a generalized formulation for kinetically controlled reactions. *Water Resources Research* **2002,** *3*, 13-11–13-21.

Mayer, K. U.; MacQuarrie, K. T. Solution of the MoMaS reactive transport benchmark with MIN3P—model formulation and simulation results. *Computational Geosciences* **2010,** *14*, 405–419.

Meakin, P.; Tartakovsky, A. M. Modeling and simulation of pore-scale multiphase fluid flow and reactive transport in fractured and porous media. *Reviews of Geophysics* **2009,** *47*.

Meeussen, J. C. ORCHESTRA: An object-oriented framework for implementing chemical equilibrium models. *Environmental Science & Technology* **2003,** *37*, 1175–1182.

Molins, S.; Mayer, K.; Scheutz, C.; Kjeldsen, P. Role of transport mechanisms in the attenuation of landfill gas in cover soils: A multicomponent modelling study. *J. Environ. Qual* **2008,** *37*, 459–468.

Molins, S.; Mayer, K. U. Coupling between geochemical reactions and multicomponent gas and solute transport in unsaturated media: A reactive transport modeling study. *Water Resources Research* **2007,** *43*. doi:https://doi.org/10.1029/2006WR005206

Molins, S.; Soulaine, C.; Prasianakis, N. I.; Abbasi, A.; Poncet, P.; Ladd, A. J.; . . . Tchelepi, H. A. Simulation of mineral dissolution at the pore scale with evolving fluid-solid interfaces: Review of approaches and benchmark problem set. *Computational Geosciences* **2021,** *25*, 1285–1318.

Molins, S.; Trebotich, D.; Arora, B.; Steefel, C. I.; Deng, H. Multi-scale model of reactive transport in fractured media: diffusion limitations on rates. *Transport in Porous Media* **2019,** *128*, 701–721.

Molins, S.; Trebotich, D.; Miller, G. H.; Steefel, C. I. Mineralogical and transport controls on the evolution of porous media texture using direct numerical simulation. *Water Resources Research* **2017,** *53*, 3645–3661. doi:https://doi.org/10.1002/2016WR020323

Molins, S.; Trebotich, D.; Steefel, C. I.; Shen, C. An investigation of the effect of pore scale flow on average geochemical reaction rates using direct numerical simulation. *Water Resources Research* **2012,** *48*. doi:https://doi.org/10.1029/2011WR011404

Molins, S.; Trebotich, D.; Yang, L.; Ajo-Franklin, J. B.; Ligocki, T. J.; Shen, C.; Steefel, C. I. Pore-Scale Controls on Calcite Dissolution Rates from Flow-through Laboratory and Numerical Experiments. *Environmental Science & Technology* **2014,** *48*, 7453–7460. doi:10.1021/es5013438

Müller, I. On the entropy inequality. *Archive for Rational Mechanics and Analysis* **1967,** *26*, 118–141.

Navarre-Sitchler, A. K.; Maxwell, R. M.; Siirila, E. R.; Hammond, G. E.; Lichtner, P. C. Elucidating geochemical response of shallow heterogeneous aquifers to CO_2 leakage using high-performance computing: Implications for monitoring of CO_2 sequestration. *Advances in Water Resources* **2013,** *53*, 45–55. doi:https://doi.org/10.1016/j.advwatres.2012.10.005

Newell, D. L.; Carey, J. W.; Backhaus, S. N.; Lichtner, P. Experimental study of gravitational mixing of supercritical CO_2. *International Journal of Greenhouse Gas Control* **2018,** *71*, 62–73. doi:https://doi.org/10.1016/j.ijggc.2018.02.013

Nguyen, B. N.; Hou, Z.; Bacon, D. H.; Murray, C. J.; White, M. D. Three-dimensional modeling of the reactive transport of CO_2 and its impact on geomechanical properties of reservoir rocks and seals. *International Journal of Greenhouse Gas Control* **2016,** *46*, 100–115. doi:https://doi.org/10.1016/j.ijggc.2016.01.004

Noiriel, C.; Luquot, L.; Madé, B.; Raimbault, L.; Gouze, P.; van der Lee, J. Changes in reactive surface area during limestone dissolution: an experimental and modelling study. *Chemical Geology* **2009,** *265*, 160–170. https://doi.org/10.1016/j.chemgeo.2009.01.032

Noiriel, C.; Soulaine, C. Pore-Scale Imaging and Modelling of Reactive Flow in Evolving Porous Media: Tracking the Dynamics of the Fluid–Rock Interface. *Transport in Porous Media* **2021,** *140*, 181–213. doi:10.1007/s11242-021-01613-2

Nordstrom, D. K.; Alpers, C. N.; Ptacek, C. J.; Blowes, D. W. Negative pH and Extremely Acidic Mine Waters from Iron Mountain, California. *Environmental Science & Technology* **2000,** *34*, 254–258. doi:10.1021/es990646v

Oostrom, M.; Rockhold, M. L.; Thorne, P. D.; Truex, M. J.; Last, G. V.; Rohay, V. J. Carbon Tetrachloride Flow and Transport in the Subsurface of the 216-Z-9 Trench at the Hanford Site. *Vadose Zone Journal* **2007,** *6*, 971–984. doi:https://doi.org/10.2136/vzj2006.0166

Oostrom, M.; Wietsma, T. W.; Strickland, C. E.; Freedman, V. L.; Truex, M. J. Sensor and Numerical Simulator Evaluation for Porous Medium Desiccation and Rewetting at the Intermediate Laboratory Scale. *Vadose Zone Journal* **2012,** *11*. doi:https://doi.org/10.2136/vzj2011.0089

Parkhurst, D. L.; Appelo, C. Description of input and examples for PHREEQC version 3—a computer program for speciation, batch-reaction, one-dimensional transport, and inverse geochemical calculations. *US geological survey techniques and methods* **2013,** *6*, 497.

Parmigiani, A.; Huber, C.; Bachmann, O.; Chopard, B. Pore-scale mass and reactant transport in multiphase porous media flows. *Journal of Fluid Mechanics* **2011,** *686*, 40–76. doi:10.1017/jfm.2011.268

Pfeiffer, W.; Graupner, B.; Bauer, S. The coupled non-isothermal, multiphase-multicomponent flow and reactive transport simulator OpenGeoSys–ECLIPSE for porous media gas storage. *Environmental Earth Sciences* **2016,** *75*, 1–15.

Prasianakis, N. I.; Curti, E.; Kosakowski, G.; Poonoosamy, J.; Churakov, S. V. Deciphering pore-level precipitation mechanisms. *Scientific Reports* **2017,** *7*, 13765. doi:10.1038/s41598-017-14142-0

Pruess, K. The TOUGH Codes—A Family of Simulation Tools for Multiphase Flow and Transport Processes in Permeable Media. *Vadose Zone Journal* **2004,** *3*, 738–746. doi:10.2113/3.3.738

Quintard, M.; Whitaker, S. Dissolution of an immobile phase during flow in porous media. *Industrial & Engineering Chemistry Research* **1999,** *38*, 833–844.

Schoenberg, I. J. Contributions to the problem of approximation of equidistant data by analytic functions. Part A. *Quarterly of Applied Mathematics* **1946,** *4*, 45–99.

Shao, H.; Dmytrieva, S. V.; Kolditz, O.; Kulik, D. A.; Pfingsten, W.; Kosakowski, G. Modeling reactive transport in non-ideal aqueous–solid solution system. *Applied Geochemistry* **2009,** *24*, 1287–1300.

Shao, H.; Kosakowski, G.; Berner, U.; Kulik, D. A.; Mäder, U.; Kolditz, O. Reactive transport modeling of the clogging process at Maqarin natural analogue site. *Physics and Chemistry of the Earth, Parts A/B/C* **2013,** *64*, 21–31.

Shao, H.; Kulik, D. A.; Berner, U.; Kosakowski, G.; Kolditz, O. Modeling the competition between solid solution formation and cation exchange on the retardation of aqueous radium in an idealized bentonite column. *Geochemical Journal* **2009,** *43*, e37–e42.

Singh, A.; Delfs, J. O.; Görke, U. J.; Kolditz, O. Toward physical aspects affecting a possible leakage of geologically stored CO_2 into the shallow subsurface. *Acta Geotechnica* **2014,** *9*, 81–86.

Singleton, M. J.; Sonnenthal, E. L.; Conrad, M. E.; DePaolo, D. J.; Gee, G. W. Multiphase reactive transport modeling of seasonal infiltration events and stable isotope fractionation in unsaturated zone pore water and vapor at the Hanford site. *Vadose Zone Journal* **2004,** *3*, 775–785.

Slattery, J. C. *Advanced transport phenomena*; Cambridge University Press, 1999.

Sonnenthal, E.; Spycher, N. Drift-scale coupled processes model: analysis and model report; (AMR) N0120/U0110; Yucca Mountain Nuclear Waste Disposal Project; Lawrence Berkeley National Laboratory: Berkeley, CA, 2000.

Soulaine, C.; Pavuluri, S.; Claret, F.; Tournassat, C. porousMedia4Foam: Multi-scale open-source platform for hydro-geochemical simulations with OpenFOAM®. *Environmental Modelling & Software* **2021,** *145*, 105199. doi:https://doi.org/10.1016/j.envsoft.2021.105199

Soulaine, C.; Roman, S.; Kovscek, A.; Tchelepi, H. A. Mineral dissolution and wormholing from a pore-scale perspective. *Journal of Fluid Mechanics* **2017,** *827*, 457–483. doi:10.1017/jfm.2017.499

Soulaine, C.; Tchelepi, H. A. Micro-continuum Approach for Pore-Scale Simulation of Subsurface Processes. *Transport in Porous Media* **2016,** *113*, 431–456. doi:10.1007/s11242-016-0701-3

Spycher, N.; Sonnenthal, E.; Apps, J. Fluid flow and reactive transport around potential nuclear waste emplacement tunnels at Yucca Mountain, Nevada. *Journal of Contaminant Hydrology* **2003,** *62*, 653–673.

Starchenko, V.; Ladd, A. J. C. The Development of Wormholes in Laboratory-Scale Fractures: Perspectives From Three-Dimensional Simulations. *Water Resources Research* **2018,** *54*, 7946–7959. doi:https://doi.org/10.1029/2018WR022948

Starchenko, V.; Marra, C. J.; Ladd, A. J. C. Three-dimensional simulations of fracture dissolution. *Journal of Geophysical Research: Solid Earth* **2016,** *121*, 6421–6444. doi:https://doi.org/10.1002/2016JB013321

Steefel, C.; Lichtner, P. Multicomponent reactive transport in discrete fractures: II: Infiltration of hyperalkaline groundwater at Maqarin, Jordan, a natural analogue site. *Journal of Hydrology* **1998,** *209*, 200–224.

Steefel, C. I.; Appelo, C. A. J.; Arora, B.; Jacques, D.; Kalbacher, T.; Kolditz, O.; . . . Yeh, G. T. Reactive transport codes for subsurface environmental simulation. *Computational Geosciences* **2015,** *19*, 445–478. doi:10.1007/s10596-014-9443-x

Steefel, C. I.; Beckingham, L. E.; Landrot, G. Micro-Continuum Approaches for Modeling Pore-Scale Geochemical Processes. *Reviews in Mineralogy and Geochemistry* **2015,** *80*, 217–246. doi:10.2138/rmg.2015.80.07

Steefel, C. I.; Molins, S. *CrunchFlow. Software for modeling multicomponent reactive flow and transport*; User's manual; Lawrence Berkeley National Laboratory: Berkeley, CA, 2009.

Strang, G. On the Construction and Comparison of Difference Schemes. *SIAM Journal on Numerical Analysis* **1968,** *5*, 506–517. doi:10.1137/0705041

Su, D.; Mayer, K.; MacQuarrie, K. *Reactive Transport Modelling Investigation of Elevated Dissolved Sulphide Concentrations in Sedimentary Basin Rocks*; NWMO Technical Report, NWMO-TR-2018-07; 2018.

Su, D.; Mayer, K. U.; MacQuarrie, K. T. Parallelization of MIN3P-THCm: A high performance computational framework for subsurface flow and reactive transport simulation. *Environmental Modelling & Software* **2017,** *95*, 271–289.

Su, D.; Mayer, K. U.; MacQuarrie, K. T. B. MIN3P-HPC: A High-Performance Unstructured Grid Code for Subsurface Flow and Reactive Transport Simulation. *Mathematical Geosciences* **2021,** *53*, 517–550. doi:10.1007/s11004-020-09898-7

Tartakovsky, A. M.; Meakin, P. A smoothed particle hydrodynamics model for miscible flow in three-dimensional fractures and the two-dimensional Rayleigh–Taylor instability. *Journal of Computational Physics* **2005,** *207*, 610–624. doi:https://doi.org/10.1016/j.jcp.2005.02.001

Tartakovsky, A. M.; Meakin, P.; Scheibe, T. D.; Eichler West, R. M. Simulations of reactive transport and precipitation with smoothed particle hydrodynamics. *Journal of Computational Physics* **2007a,** *222*, 654–672. doi:https://doi.org/10.1016/j.jcp.2006.08.013

Tartakovsky, A. M.; Meakin, P.; Scheibe, T. D.; Wood, B. D. A smoothed particle hydrodynamics model for reactive transport and mineral precipitation in porous and fractured porous media. *Water Resources Research* **2007b,** *43*. doi:https://doi.org/10.1029/2005WR004770

Tartakovsky, A. M.; Redden, G.; Lichtner, P. C.; Scheibe, T. D.; Meakin, P. Mixing-induced precipitation: Experimental study and multiscale numerical analysis. *Water Resources Research* **2008,** *44*. doi:https://doi.org/10.1029/2006WR005725

Tartakovsky, A. M.; Trask, N.; Pan, K.; Jones, B.; Pan, W.; Williams, J. R. Smoothed particle hydrodynamics and its applications for multiphase flow and reactive transport in porous media. *Computational Geosciences* **2016,** *20*, 807–834. doi:10.1007/s10596-015-9468-9

Tian, Z.; Xing, H.; Tan, Y.; Gu, S.; Golding, S. D. Reactive transport LBM model for CO_2 injection in fractured reservoirs. *Computers & Geosciences* **2016,** *86*, 15–22.

Trebotich, D.; Straalen, B. V.; Graves, D.; Colella, P. Performance of embedded boundary methods for CFD with complex geometry. *Journal of Physics: Conference Series* **2008,** *125*, 012083. doi:10.1088/1742-6596/125/1/012083

Truesdell, C.; Noll, W. *The Non-linear Field Theories of Mechanics*; Springer-Verlag: Berlin (1965 & 1992); 1992.

Tutolo, B. M.; Kong, X.-Z.; Seyfried, W. E.; Saar, M. O. High performance reactive transport simulations examining the effects of thermal, hydraulic, and chemical (THC) gradients on fluid injectivity at carbonate CCUS reservoir scales. *International Journal of Greenhouse Gas Control* **2015,** *39*, 285–301. doi:https://doi.org/10.1016/j.ijggc.2015.05.026

Vafai, K.; Tien, C. L. Boundary and inertia effects on flow and heat transfer in porous media. *International Journal of Heat and Mass Transfer* **1981,** *24*, 195–203.

Verma, A.; Pruess, K. Thermohydrological conditions and silica redistribution near high-level nuclear wastes emplaced in saturated geological formations. *Journal of Geophysical Research: Solid Earth* **1988,** *93*, 1159–1173. https://doi.org/10.1029/JB093iB02p01159

Vriens, B.; Seigneur, N.; Mayer, K. U.; Beckie, R. D. Scale dependence of effective geochemical rates in weathering mine waste rock. *J Contam Hydrol* **2020,** *234*, 103699. doi:10.1016/j.jconhyd.2020.103699

Wang, W.; Kolditz, O. Object-oriented finite element analysis of thermo-hydro-mechanical (THM) problems in porous media. *International Journal for Numerical Methods in Engineering* **2007,** *69*, 162-201.

Wanner, C.; Druhan, J. L.; Amos, R. T.; Alt-Epping, P.; Steefel, C. I. Benchmarking the simulation of Cr isotope fractionation. *Computational Geosciences* **2015,** *19*, 497–521. doi:10.1007/s10596-014-9436-9

Wanner, C.; Eggenberger, U.; Mäder, U. A chromate-contaminated site in southern Switzerland–Part 2: Reactive transport modeling to optimize remediation options. *Applied Geochemistry* **2012,** *27*, 655–662.

Wanner, C.; Sonnenthal, E. L. Assessing the control on the effective kinetic Cr isotope fractionation factor: A reactive transport modeling approach. *Chemical Geology* **2013,** *337*, 88–98.

Ward, A. L.; White, M. D.; Freeman, E. J.; Zhang, Z. *STOMP Subsurface Transport Over Multiple Phase Addendum: Sparse Vegetation Evapotranspiration Model for the Water-Air-Energy Operational Mode*; PNNL-15465; Pacific Northwest National Laboratory: Richland, WA; 2005.

White, M.; Oostrom, M. *STOMP Subsurface Transport Over Multiple Phases: User's guide*; PNNL-11218; Pacific Northwest National Laboratory: Richland, WA; 1997.

White, M.; Oostrom, M. *STOMP: Subsurface transport over multiple phases. Theory guide*; PNNL-12030; Pacific Northwest National Laboratory: Richland, WA; 2000.

White, M.; Oostrom, M. *STOMP subsurface transport over multiple phases, version 4.0, user's guide*; PNNL-15782; Pacific Northwest National Laboratory, Richland, WA; 2006.

White, M. D.; Bacon, D. H.; McGrail, B. P.; Watson, D. J.; White, S. K.; Zhang, Z. *STOMP subsurface transport over multiple phases: STOMP-CO2 and STOMP-CO2e guide: version 1.0*; Pacific Northwest National Laboratory, Richland, WA; 2012.

White, M. D.; Kneafsey, T. J.; Seol, Y.; Waite, W. F.; Uchida, S.; Lin, J. S.; . . . Zyrianova, M. An international code comparison study on coupled thermal, hydrologic and geomechanical processes of natural gas hydrate-bearing sediments. *Marine and Petroleum Geology* **2020,** *120*, 104566. doi:https://doi.org/10.1016/j.marpetgeo.2020.104566

White, M. D.; McGrail, B. P. *STOMP Subsurface Transport Over Multiple Phases version 1.0 Addendum: ECKEChem Equilibrium-Conservation-Kinetic Equation Chemistry and reactive transport*; PNNL-15482; Pacific Northwest National Laboratory: Richland, WA; 2005.

White, M. D.; McPherson, B. J.; Grigg, R. B.; Ampomah, W.; Appold, M. S. Numerical Simulation of Carbon Dioxide Injection in the Western Section of the Farnsworth Unit. *Energy Procedia* **2014,** *63*, 7891–7912. doi:https://doi.org/10.1016/j.egypro.2014.11.825

White, M. D.; Wurstner, S. K.; McGrail, B. P. Numerical studies of methane production from Class 1 gas hydrate accumulations enhanced with carbon dioxide injection. *Marine and Petroleum Geology* **2011,** *28*, 546–560. doi:https://doi.org/10.1016/j.marpetgeo.2009.06.008

Wolf-Gladrow, D. A. *Lattice-Gas Cellular Automata and Lattice Boltzmann Models An Introduction*, 1st ed., 2000. ed.; Springer Berlin Heidelberg: Berlin, Heidelberg, 2000.

Xie, M.; Bauer, S.; Kolditz, O.; Nowak, T.; Shao, H. Numerical simulation of reactive processes in an experiment with partially saturated bentonite. *Journal of Contaminant Hydrology* **2006,** *83*, 122–147.

Xie, M.; Kolditz, O.; Moog, H. C. A geochemical transport model for thermo-hydro-chemical (THC) coupled processes with saline water. *Water Resources Research* **2011,** *47*.

Xie, M.; Mayer, K. U.; Claret, F.; Alt-Epping, P.; Jacques, D.; Steefel, C.; . . . Simunek, J. Implementation and evaluation of permeability-porosity and tortuosity-porosity relationships linked to mineral dissolution-precipitation. *Computational Geosciences* **2015,** *19*, 655–671. doi:10.1007/s10596-014-9458-3

Xie, M.; Rasouli, P.; Mayer, K.; MacQuarrie, K. *Reactive Transport Modelling in Low Permeability Media – MIN3P-THCm Simulations of EBS TF-C Compacted Bentonite Diffusion Experiments*; Technical Report NWMO-TR-2014-23; 2014.

Xu, T.; Apps, J. A.; Pruess, K. Numerical simulation of CO_2 disposal by mineral trapping in deep aquifers. *Applied Geochemistry* **2004,** *19*, 917–936.

Xu, T.; Apps, J. A.; Pruess, K. Reactive geochemical transport simulation to study mineral trapping for CO_2 disposal in deep arenaceous formations. *Journal of Geophysical Research: Solid Earth* **2003a,** *108*(B2).

Xu, T.; Sonnenthal, E.; Bodvarsson, G. A reaction-transport model for calcite precipitation and evaluation of infiltration fluxes in unsaturated fractured rock. *Journal of Contaminant Hydrology* **2003b,** *64*, 113–127.

Xu, T.; Sonnenthal, E.; Spycher, N.; Pruess, K. TOUGHREACT—a simulation program for non-isothermal multiphase reactive geochemical transport in variably saturated geologic media: applications to geothermal injectivity and CO_2 geological sequestration. *Computers & Geosciences* **2006,** *32*, 145–165.

Xu, T.; Sonnenthal, E.; Spycher, N.; Pruess, K.; Brimhall, G.; Apps, J. Modeling multiphase non-isothermal fluid flow and reactive geochemical transport in variably saturated fractured rocks: 2. Applications to supergene copper enrichment and hydrothermal flows. *American Journal of Science* **2001,** *301*, 34–59.

Xu, T.; Sonnenthal, E.; Spycher, N.; Zheng, L. *TOUGHREACT V3. 0-OMP reference manual: A parallel simulation program for non-isothermal multiphase geochemical reactive transport*; University of California, Berkeley, 2014.

Yeh, G.; Li, Y.; Jardine, P.; Burgos, W.; Fang, Y.; Li, M.; Siegel, M. *HYDROGEOCHEM 4.0: A coupled model of fluid flow, thermal transport, and HYDROGEOCHEM-ical transport through saturated unsaturated media, Version 4.0;* ORNL/TM-2004/103; 2004; 37831.

Yoon, H.; Oostrom, M.; Wietsma, T. W.; Werth, C. J.; Valocchi, A. J. Numerical and experimental investigation of DNAPL removal mechanisms in a layered porous medium by means of soil vapor extraction. *Journal of Contaminant Hydrology* **2009,** *109*, 1–13.

Zhang, M.; Zhang, Y.; Lichtner, P. Evaluating model complexity in simulating supercritical CO_2 dissolution, leakage, footprint, and reservoir pressure for three-dimensional hierarchical aquifer. *International Journal of Greenhouse Gas Control* **2017,** *64*, 284–299. doi:https://doi.org/10.1016/j.ijggc.2017.07.022

Zhu, Y.; Fox, P. J. Simulation of Pore-Scale Dispersion in Periodic Porous Media Using Smoothed Particle Hydrodynamics. *Journal of Computational Physics* **2002,** *182*, 622–645. doi:https://doi.org/10.1006/jcph.2002.7189

Zhu, Y.; Fox, P. J. Smoothed Particle Hydrodynamics Model for Diffusion through Porous Media. *Transport in Porous Media* **2001,** *43*, 441–471. doi:10.1023/A:1010769915901

Ziegler, H. *An Introduction to Thermomechanics*, 2nd Rev. ed.; North-Holland Publishing Company: Amsterdam, 1983.

APPENDIX

Expressions of reaction-induced porosity and permeability changes implemented in the reactive transport codes.

- Power law

$$k = k_0 \left(\frac{\phi}{\phi_0}\right)^n \tag{A.1}$$

- Kozeny-Carman

$$k = k_0 \left(\frac{\phi}{\phi_0}\right)^n \left(\frac{1-\phi_0}{1-\phi}\right)^m \tag{A.2}$$

by default, $n = 2$ and $m = 3$ (Kozeny, 1927; Carman, 1937).

- Verma-Pruess

$$k = k_0 \left(\frac{\phi - \phi_c}{\phi_0 - \phi_c}\right)^n \tag{A.3}$$

n is a model parameter. ϕ_c refers to the critical porosity where permeability reduces to 0 (Verma and Pruess, 1988).

- Hele-Shaw

$$k = \frac{h^2}{12} \tag{A.4}$$

for simulating 2D depth-averaged flow in micromodels; h is the gap between the two plates.

Expressions of some specific surface area models implemented in porousMedia4Foam

- Volume of solid

$$A_s = |\nabla Y_s| \psi \tag{A.5}$$

compute the local surface area based on the mineral mapping. ψ is a diffuse interface function.

- Power-law

$$A_s = A_0 (Y_s)^n \tag{A.6}$$

n is a user defined variable.

- Sugar lump

$$A_s = \left(A_0 + A_m \left(1 - \left(\frac{Y_s}{Y_0}\right)^{n_1}\right)^{n_2}\right)\left(\frac{Y_s}{Y_0}\right)^{n_3} \tag{A.7}$$

A_m is the maximum surface area given by the sum of the surface areas of all individual particles. Parameters n_1, n_2, and n_3 are user-defined parameters (Noiriel et al., 2009).

- Hydro-geochemical coupling

$$A_s = A_0 \left(\frac{Y_s}{Y_0}\right)^n \left(1 - \exp\left(Pe^{-p} Da^{-q}\right)\right) \tag{A.9}$$

n, p, q are user defined parameters (Soulaine et al., 2017); Pe and Da are Péclet and Damkhöler numbers.

Expressions of some of the dispersion models implemented in the reactive transport codes:

- Diffusion only

$$D_i^* = D_i I \tag{A.10}$$

- Archie's Law

$$D_i^* = \phi^n D_i I \tag{A.11}$$

- Linear dispersion

$$D_i^* = \phi^n \left((D_i + \alpha_T |\mathbf{u}|) I + \frac{(\alpha_L - \alpha_T)}{|\mathbf{u}|} \mathbf{u}\mathbf{u} \right) \tag{A.12}$$

Tortuosity is represented by ϕ^n. α_T and α_L are model parameters describing lateral and longitudinal dispersion, respectively. I is the matrix/tensor identity.

Brian Anderson
Director
National Energy Technology Laboratory
U.S. Department of Energy

John Wimer
Acting Chief Research Officer
Science & Technology Strategic Plans
& Programs
National Energy Technology Laboratory
U.S. Department of Energy

Bryan Morreale
Associate Laboratory Director for
Research & Innovation
Research & Innovation Center
National Energy Technology Laboratory
U.S. Department of Energy